CHARACTERISTIC X-RAY PRODUCTION

BY

HEAVY ION-ATOM COLLISIONS

F. W. SARIS

CHARACTERISTIC X-RAY PRODUCTION

BY

HEAVY ION-ATOM COLLISIONS

CHARACTERISTIC X-RAY PRODUCTION

BY

HEAVY ION-ATOM COLLISIONS

PROEFSCHRIFT

TER VERKRIJGING VAN DE GRAAD VAN DOCTOR IN DE WISKUNDE EN NATUURWETENSCHAPPEN AAN DE RIJKS-UNIVERSITEIT TE LEIDEN, OP GEZAG VAN DE RECTOR MAGNIFICUS DR. C. SOETEMAN, HOOGLERAAR IN DE FACULTEIT DER LETTEREN, TEN OVERSTAAN VAN EEN COMMISSIE UIT DE SENAAT TE VERDEDIGEN OP WOENSDAG 3 MAART 1971 TE KLOKKE 15.15 UUR

DOOR

FRANS WILLEM SARIS

GEBOREN TE LEIDEN IN 1942

Promotor: Prof.Dr. J. Kistemaker

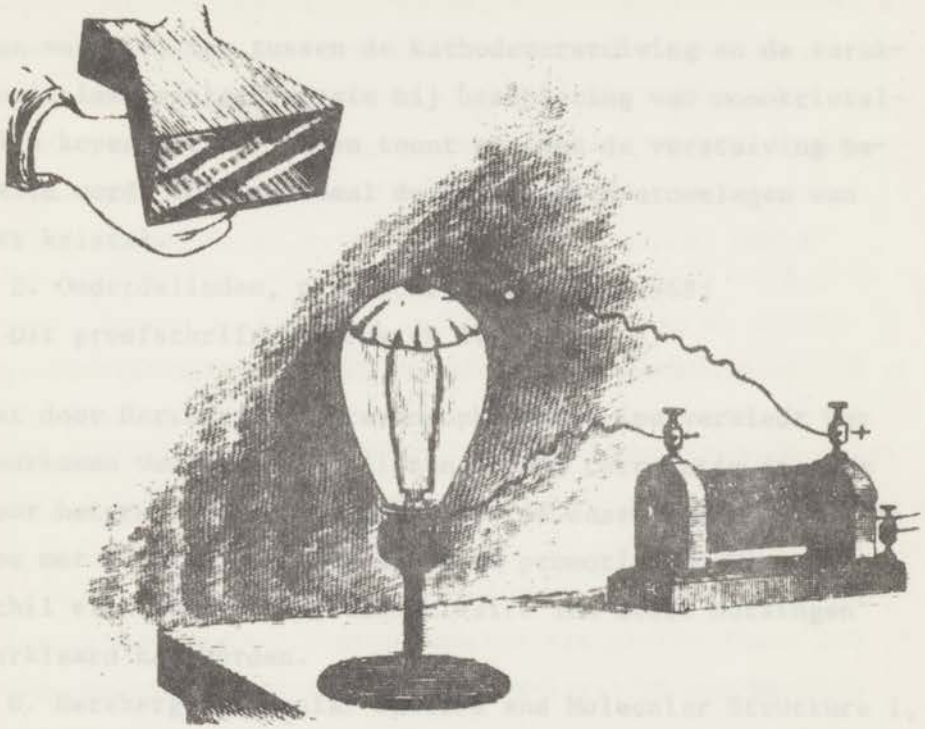

X RAY EXPERIMENT SIMPLIFIED.

aan mijn ouders

aan Pien en onze kinderen

S T E L L I N G E N

1. Een vergelijking tussen de kathodeverstuiving en de karakteristieke röntgenemissie bij beschieting van monokristallijn koper met Ar^+ ionen toont aan dat de verstuiving bepaald wordt door maximaal de eerste tien atoomlagen van het kristal.

   D. Onderdelinden, proefschrift, Leiden 1968;
   Dit proefschrift, hoofdstuk IV.

2. Het door Herzberg beschreven opbouwprincipe verbiedt het voorkomen van snijdende lijnen in een correlatie diagram voor heternucleaire systemen. Het is daarom niet duidelijk hoe met het Fano-Lichten model de promotie van binnenschil elektronen in heteronucleaire ion-atoom botsingen verklaard kan worden.

   G. Herzberg, Molecular Spectra and Molecular Structure I, Spectra of Diatomic Molecules, D. van Nostrand, Inc., (Princeton N.J., 1950);
   W. Fano, W. Lichten, Phys.Rev.Letters 14 (1965) 627.

3. De inelastische component van het stoppend vermogen voor ionen in de vaste stof vertoont een karakteristieke afhankelijkheid van het atoomgetal Z van het projectiel. Er bestaat een relatie tussen deze Z afhankelijkheid en die voor de werkzame doorsneden voor röntgenemissie bij ionenbeschieting van de vaste stof.

4. Hoewel de vacuumtechnologie ver genoeg ontwikkeld is om de verontreiniging van een schoon oppervlak te kunnen voorkomen, moeten de fysische technieken nog ontwikkeld worden om zo'n schoon oppervlak te produceren en op verontreinigingen te controleren.

   Proceedings International NEVAC Symposium "The Solid-Vacuum Interface", Ned.Tijdschr.v.Vac.Techniek 8 (1970) 406.

5. Bij de studie van hyperfijninteracties verschaft de combinatie van channeling en karakteristieke röntgenemissie een onafhankelijke methode voor het bepalen van de fractie substitutionele gastatomen in alle mogelijke metalen.

   Proc.Roy.Soc. A311 (1969) 1-209.

6. Het heeft weinig zin berekeningen uit te voeren over de afwijking van de regel van Mathiessen tengevolge van magnetische gastatomen in een metaal, zolang voor de afwijking tengevolge van niet-magnetische gastatomen nog geen bevredigende verklaring is gevonden.

   B. Lengeler, W. Schilling, H. Wenzl, Journ.Low Temp.Phys. 2 (1970) 237;

   M.J. Rice, O. Bance, Phys.Rev. B2 (1970) 3833.

7. In het model van Morehead Jr. en Crowder voor het vormen van amorf silicium door ionenbombardement wordt de rekristallisatie warmte ten onrechte buiten beschouwing gelaten.

   F.F. Morehead Jr., B.L. Crowder, Rad.Effects 6 (1970) 27.

8. De resultaten van Adair en McClurg voor het thermomagnetische koppel in NH_3 zijn, in tegenstelling tot hun mening, een bevestiging van de verklaring van de resultaten voor het viscomagnetische effect in NH_3.

   T.W. Adair, G.R. McClurg, Phys.Rev. A2 (1970) 1968;
   J. Korving, Physica 46 (1970) 619.

9. Een verregaande democratisering van de Stichting F.O.M. dient vooraf te gaan aan een vergroting van de tweede geldstroom die door deze stichting gestuurd wordt.

10. Het verdient de voorkeur om tijdens de promotie de discussies over stellingen te vervangen door een gedachtenwisseling over de wetenschappelijke, technologische en sociale merites van het in het proefschrift beschreven onderzoek.

    A. Weinberg, Criteria for Scientific Choice, Physics Today, March 1964, p.42.

F.W. Saris,
3 maart 1971.

CONTENTS

CHAPTER I

GENERAL INTRODUCTION AND SURVEY

1. *Introduction.* The production of characteristic X-rays by electron or photon bombardment of a target is a familiar phenomenon. If the impact removes an electron from an innershell then the subsequent rearrangement process may produce a photon with an energy characteristic of the element bombarded. Besides electrons or photons also heavy charged particles may be employed for X-ray production. A striking phenomenon during violent encounters between atomic particles is the highly inelastic character of the collision, i.e. kinetic energy is transferred into excitation and ionization of the colliding particles. The inelasticity of ion-atom encounters has been studied extensively in the past decade [1]. The early data on collisions of Ar^+ + Ar and Ne^+ + Ne suggested vacancies to be created in the innershells of the colliding particles. In 1965 an innershell excitation mechanism was proposed, based upon molecular orbital promotion, an idea which became known as the Fano-Lichten model [2]. The authors also suggested a search for fast electrons originating from Auger transitions to the innershell vacancies, a

suggestion which was promptly verified [3]. However, the innershell vacancy creation may also initiate a radiative decay, therefore we started to look for Ar L-shell and Ne K-shell X-ray emission. This resulted in measuring total cross sections in collisions of Ar^+, Ne^+, H^+ on Ar and Ne^+ on Ne, see chapter II. From the data we inferred critical internuclear distances for innershell vacancy creation and the probability of a radiative decay process. We anticipated a strong influence of the innershell excitation in ion-atom collisions upon the kind of projectile. This influence is emphasized in chapter III, where various heteronuclear collisions on argon are investigated.

So far we have only mentioned atomic collision studies in the gas phase, whereas in recent years much progress has been achieved, particularly in the field of X-ray production, by using solid targets. At keV energies the collision time is 2 to 3 orders of magnitude smaller than the vibration time of the atoms in a lattice. Moreover in order to excite an innershell the critical distance between projectile and target atom is generally an order of magnitude smaller than the interatomic spacing in the lattice. So when studying violent atomic collisions in solids one is inclined to consider the solid simply as a very dense gaseous target. Indeed there are many analogies between interactions of fast ions with gases and solids, but also differences are observed. Here it is appropriate to refer to the work of Snoek [4] and Van der Weg [5]. The underlying thesis and especially the work described in chapter IV forms a natural follow up of the particle solid interaction studies of our group.

The scope of chapter IV is two-fold. The X-ray production by Ar^+ and Ne^+ bombardment of copper has been measured and is compared to collisions in the gas phase. On the other hand the penetration and entrapment of Ar^+ and Ne^+ into the monocrystalline copper target has been studied by making use of the ion induced X-ray emission. Following chapter IV are conclusions along with possible extensions that may be derived from the work described in this thesis. The introduction is continued by a general survey of the literature aiming to show that in recent years the detection and analysis of X-rays contributed substantially to the understanding of ion-atom collision processes.

2. *Experimental.* A mass- and energy analyzed ion beam impinges on a target. The emitted soft X-rays are identified in a thin window proportional counter operated in flow mode. If a gaseous target is being used then the X-ray emission cross section σ_{em} is defined by:

$$\sigma_{em} = \frac{I}{N_i \, A \, \Omega \, n \, L} \qquad (1)$$

I is the detector signal, measured as a number of counts; N_i is the number of incident ions; A is the efficiency factor of the photodetection system; Ω is the geometrical correction factor; n is the target density; L is the interaction length viewed by the proportional counter. The cross section has the dimension of an area. The apparatus and experimental method used in our experiments are generally identical to those of other investigators and are described in detail in chapter II. Instead of a gaseous target many groups have used a solid target in their

X-ray experiments. Then the X-ray production cross section σ_{em} for a given projectile energy E can be evaluated from the thick target yield N_{ph} by the relation:

$$\sigma_{em} = \frac{1}{n} \frac{dN_{ph}}{dE} S + \frac{\mu}{n} N_{ph} \qquad (2)$$

S is the target stopping power, μ is its absorption coefficient for the relevant photons. Eq. (2) has been derived by Merzbacher and Lewis in their review paper (ref. 2) on X-ray production by proton or alpha particle irradiation of solid targets. Recently also the thick target yield of X-rays under heavy ion bombardment is reduced to the emission cross section by the use of eq. (2). Some disadvantages of this procedure will be discussed in chapter IV.

2.1. Cross section data. Innershell ionization and X-ray production by proton impact have received much attention in the theoretical work of Merzbacher and Lewis [6], Bang and Hansteen [7] and more recently Garcia [8] and Hansteen and Mosebekk [8]; and in the experimental work of Khan's group [9]. References and data on X-ray emission cross sections in heavy ion-atom collisions are listed in table I, see page 19. The present data on X-ray emission cross sections in heavy ion-atom collisions have yielded the answer to a recent question raised by Fano [23]: "Do proton impacts differ substantially from those of electron-carrying ions?". The mechanism responsible for the innershell excitation by proton impact is believed to be a direct Coulomb interaction between the proton and the innershell electron involved. A classical binary

encounter model is found to be in good agreement with experiment [8]. In comparison with these cross sections, the cross sections in heavy ion-atom collisions are 3 to 5 orders of magnitude higher, see ref. 10, 12, 14, 21 and chapters II and III. Only one exception [18]: the cross section for Cu-K X-ray production in collisions of protons on Cu is found to be higher than for oxygen on Cu. Generally it is observed that each atomic shell gets readily excited when the collision forces an interpenetration of shells of comparable binding energy, thus giving large cross sections. It is supposed that during the collision a short-lived quasi-molecule is formed and innershell electrons are promoted because energy level crossings occur as the projectile approaches the target atom close enough [2]. In conclusion: the innershell excitation mechanism in heavy ion-atom collisions appears to be different from proton impact.

It is interesting to note that the above conclusion is already anticipated by Tanaka and Nonaka in their work on "Production of X-rays by High Speed Argon Ions" in 1937, ref. 24. They also noticed a shell effect on the relative number of photons emitted in their experiments. In 1965 Specht [22] provided the first systematic outline of the dependence of the X-ray emission cross section on the overlap of innershells involved. He studied X-ray emission from collisions of energetic fission fragments on metal targets.

We investigated the influence of the projectile atomic number Z on the cross section for Ar L-shell X-ray emission in collisions of $Z^+ \rightarrow Ar$, see chapters III and V.

Also the Z-dependence of Cu L-shell X-ray emission has been studied in collisions of $Z^+ \rightarrow Cu$ [19,20] or $Cu^+ \rightarrow Z$ [20]. One can summarize the results so far by stating that: in a plot of the cross section versus the atomic number maxima occur for symmetrical cases and quasi-symmetrical cases, where the binding energy of the innershell under study is about equal to the binding energy of one of the innershells of the collision partners. A correlation between the observations of the outer- and innershell excitation is suggested in chapter V.

2.2. The fluorescence yield. Historically the fluorescence yield of an element has been defined in terms of the intensity of fluorescent radiation produced when a sample was exposed to a beam of energetic X-rays. More recently, it has been defined in terms of the probability that a vacancy in a given shell results in a radiative transition [25]. An Auger transition may also occur giving rise to the emission of outershell electrons. The fluorescence yield can be deduced from the X-ray emission cross section and the Auger excitation cross section of the innershell involved, see chapter II. It is observed that the fluorescence yield is influenced by the mechanism for primary vacancy creation. By comparing our Ar-L X-ray emission cross section with the Auger excitation cross section of Rudd's group [26,27], we have determined the mean Ar L-shell fluorescence yield, $\bar{\omega}_L \simeq 10^{-3}$. For proton impact on Ar the fluorescence yield is lower than for Ar^+ impact. Moreover as the impact energy of the argon projectile is increased also the $\bar{\omega}_L$ increases. Therefore it is concluded that: the fluorescence

yield is correlated to the degree of excitation and ionization of the outershell during the collision.

2.3. The photon spectrum. A thin window proportional counter is very useful for measuring total yields in the soft X-ray region. However, its resolution is rather poor. One is unable to see any subshell splitting or shift of the observed X-ray lines. In the ultra soft X-ray region the use of dispersive photon detection is necessary in order to increase the resolution. In the harder X-ray region a liquid nitrogen cooled Si(Li) detector can be employed. This latter detector has been used to observe K-shell X-rays produced by MeV proton and oxygen bombardment of Ni, Cu, Ca and V [18]. With a system resolution of 180 eV (FWHM) at 5.9 keV photon energy one is able to distinguish K_α from K_β lines. An interesting observation is that: relative to the proton bombardments, the K_α lines produced by oxygen bombardments are shifted ~ 50 eV, the K_β lines are shifted ~ 150 eV. The observed effect is interpreted as due to: multiple ionization of the outershell occurring during a heavy ion-atom collision simultaneously with the innershell excitation. The influence of the ionization on the shielding causes the lineshift. A similar effect in the Ar-L X-ray spectra of Ar^+ + Ar collisions has been observed using a soft X-ray spectrometer [28]. As the argon impact energy is increased from 50 to 330 keV, additional discrete lines show up and gain intensity relatively to the original Ar-L lines.

3. *Theoretical investigations.* By introducing the idea about promotion of molecular orbitals, Fano and Lichten [2] have proposed a qualitative model for the innershell excitation mechanism in heavy ion-atom collisions. The X-ray experiments have provided so many quantitative data that one has started to calculate theoretical cross sections based upon the above model. In the symmetrical case, $C^+ + C$, Fortner et al. [11] assume that the excitation probability for C K-shell vacancy production must follow the form of the Landau-Zener theory near the crossing of molecular orbitals. Although this model fits the C K-shell cross section rather well, there are severe restrictions as to its applicability. First of all, the Fano-Lichten model has been put up for symmetrical collisions only (actually Ar + Ar and Ne + Ne). No detailed calculations giving energy curves of molecular orbitals for heteronuclear systems are available. Moreover in the Landau-Zener model the promotion probability is 50% at the most, which is inconsistent with the measured data on the Ar-L vacancy production [29]. Kessel suggested a semi-empirical model in order to calculate cross sections and critical internuclear distances for innershell excitation [30]. This model is shown to be successful in the $Ar^+ + Ar$ case, see chapter II and ref. 26). Recent investigations of Fastrup et al. [29] also suggest the applicability to collisions of $Z^+ + Ar$ for $13 \leq Z \leq 19$. Applying the above model one can also deduce the critical internuclear distance for innershell excitation from the threshold of the X-ray emission cross section, see chapter III. These critical inter-

nuclear distances present a characteristic oscillation, which can be correlated to the Z-dependence of the geometrical sizes of the innershells involved. It is clear that many theoretical investigations are needed in order to give a complete account of the observed effects.

4. *Applications.* The electron induced X-ray spectrum consists of characteristic lines super imposed on a continuous background. An advantage in using ion bombardment is that the characteristic X-rays produced are free of the bremstrahlung. Moreover, the emission cross sections in heavy ion-atom collisions are large in comparison with electron impact [31]. For instance: the maximum cross section [32] for ionization of the Ar L-shell by electron impact is $3 \cdot 10^{-18}$ cm^2, multiplying by the fluorescence yield, $\bar{\omega}_L \simeq 10^{-3}$, gives an Ar-L X-ray emission cross section which is an order of magnitude lower than the cross section measured for 20 keV Ar^+ on Ar, see chapter II. So the characteristic X-ray production by heavy ion-atom collisions can very well be applied as a light source in the soft X-ray region.

Interesting applications lie also in the field of particle solid interactions. Thin oxygen and carbon films are normally present on many solid surfaces. A method based upon ion induced X-ray production offers a sensitive tool for studying the contamination of target surfaces. Oxygen surface densities of approximately 0.1 monolayer are measurable [34]. Recently Cairns et al. [35] have measured the implanted boron and antimony concentration profiles in silicon by the use of heavy ion X-ray excitation. Irradiation damage [33] and

lattice location of implanted species [37] can be studied by the so-called channeling effects technique [36]. We have used this technique in order to investigate the implantation of gallium into silicon [37]. In chapter IV an experiment is described in which the Ar^+ and Ne^+ irradiation of monocrystalline copper is studied by means of the characteristic X-ray production during irradiation. In conclusion: characteristic X-ray production by heavy ion-atom collisions is a subject of interest to many atomic physicists, moreover it has proved to be applicable also in various fields outside atomic physics.

TABLE I

X-ray	ion	energy [keV]	target	ref.
C-K	C^+	20- 80	C	10
"	N^+	"	"	"
"	O^+	"	"	"
"	Ne^+	"	"	"
"	Ar^+	"	"	"
"	Kr^+	"	"	"
"	Xe^+	"	"	"
C-K	C^+	20-1500	C	11
Ne-K	Ne^+	100- 400	Al	12
"	"	100- 200	Al(Ne)	"
"	"	125- 300	C	"
"	Ne^+	40- 100	Ne	13
Ne-K	"	100	Ar	"
Al-K	N^+	175- 300	Al	12
"	O^+	"	"	"
"	Ne^+	100-3200	"	"
"	Ar^+	175- 350	"	"
Al-K	N^{++}	70- 400	Al	14
"	O^{++}	"	"	"
"	Ar^{++}	"	"	"
Ar-L	C^+	30- 100	Ar	15
"	N^+	"	"	"
"	O^+	"	"	"
"	Al^+	"	"	"
"	Cl^+	"	"	"
"	Ti^+	"	"	"
"	Fe^+	"	"	"
"	Cu^+	"	"	"
Ar-L	Ar^+	8- 100	Ar	13
"	Ne^+	20- 100	"	"
Ar-L	Ar^+	30- 100	Cu	16
Ar-K	Ar^+	1500	Ar	17
Ca-K	O^{4+}	15000	Ca	18
V-K	"	"	V	"
Ni-K	"	"	Ni	"
Cu-L	Z^+	200	Cu	19
Cu-L	Z^+	40-1100	Cu	20
"	Cu^+	160	Z	"
Cu-K	O^{4+}	15000	Cu	18
Te-L	I	30000	Te	21
Yb-M	"	"	Yb	"
Hf-M	N^{++}	70- 400	Hf	14
"	O^{++}	"	"	"
"	Ar^{++}	"	"	"

REFERENCES

1) see the review article of Kessel, Q.C., in Case Studies in Atomic Collision Physics I (edited by E.W. McDaniel and M.R. McDowell, North-Holland Publ. Comp., London, 1969) p. 401.

2) Fano, U. and Lichten, W., Phys.Rev.Letters 14 (1965) 484.

3) Snoek, C., Geballe, R., Weg, W.F. v.d., Rol, P.K., and Bierman, D.J., Physica 31 (1965) 1553.
Kessel, Q.C., McCaughey, M.P. and Everhart, E., Phys.Rev.Letters 16 (1966) 1189, 17 (1966) 1170.
Rudd, M.E., Jorgensen Jr., T. and Volz, D.J., Phys.Rev. 151 (1966) 28.

4) Snoek, C., thesis, Amsterdam (1966).

5) Weg, W.F. v.d., thesis, Amsterdam (1969).

6) Merzbacher, E. and Lewis, H.W., in Encyclopedia of Physics (edited by S. Flügge, Springer, Berlin, 1958) 34, 166.

7) Bang, J. and Hansteen, J.M., Kgl.Danske Videnskab Selskab, Mat. - Fys.Medd., 31 no.13 (1959).

8) Garcia, J.D., Phys.Rev. A1 (1970) 280; ibid A1 (1970) 1402.
Hansteen, J.M. and Mosebekk, O.P., Z.Phys. 234 (1970) 281.

9) Khan, J.M., Potter, D.L. and Worley, R.D., Phys.Rev. 139 (1965) A1735; ibid, 145 (1966) 23.

10) Der, R.C., Kavanagh, F.M., Khan, J.M., Curry, B.P. and Fortner, R.J., Phys. Rev.Letters 24 (1970) 1037.

11) Fortner, R.J., Curry, B.P., Der, R.C., Kavanagh, F.M. and Khan, J.M., Phys. Rev. 185 (1969) 164.

12) Brandt, W. and Laubert, R., Phys.Rev.Letters 24 (1970) 1037.

13) Saris, F.W. and Onderdelinden, D., Physica 49 (1970) 441 (chapter II).

14) Needham Jr, P.B. and Sartwell, B.D., Phys.Rev.A, 2 (1970) 27.

15) Saris, F.W., Physica to be published and chapter III.

16) see chapter IV.

17) Kessel, Q.C., Rose, P.H. and Grodzins, L., Phys.Rev.Letters 22 (1969) 1031.

18) Richard, P., Morgan, I.L., Furuta, T. and Burch, D., Phys.Rev.Letters 23 (1969) 1009;
Richard, P., Bonner, T.I., Furuta, T. and Morgan, I.L., Phys.Rev. A1 (1970) 1044; and
Burch, D. and Richard, P., Phys.Rev.Letters 25 (1970) 983.

19) Cairns, J., Holloway, D.F. and Nelson, R.S., Atomic Collision Phenomena in Solids (ed. by D.W. Palmer, M.W. Thompson and P.D. Townsend, North-Holland Publ.Comp., Amsterdam, 1970).

20) Kavanagh, T.M., Cunningham, M.E., Der, R.C., Fortner, R.J., Khan, J.M., Zaharis, E.J. and Garcia, J.D., Phys.Rev.Letters 25 (1970) 1473.

21) Stein, H.J., Lutz, H.O., Mokler, P.H., Sistemich, K. and Armbruster, P., Phys.Rev.Letters 24 (1970) 701.

22) Specht, H.J., Z.Physik 185 (1965) 301.

23) Fano, U., Comments on At.and Mol.Physics 1 (1969) 1.

24) Tanaka, M. and Nonaka, I., Proc.Phys.Math.Soc.Japan 20 (1938) 33.

25) Fink, R.W., Jopson, R.C., Mark, H. and Swift, C.D., Rev.Mod.Phys. 38 (1966) 513.

26) Cacak, R.K., Kessel, Q.C. and Rudd, M.E., Phys.Rev. A2 (1970) 1327.

27) Volz, D.J. and Rudd, M.E., Phys.Rev. A2 (1970) 1395.

28) Cunningham, M.E., Der, R.C., Fortner, R.J., Kavanagh, T.M., Khan, J.M., Layne, C.B., Zaharis, E.J., Garcia, J.D., Phys.Rev. 24 (1970) 931.

29) Fastrup, B., Hermann, G. and Smith, K.J., Phys.Rev. A (to be published).

30) Kessel, Q.C., Bull.A, P.S. 14 (1969) 946 and private communication.

31) Glupe, G. and Mehlhorn, W., Phys.Rev.Letters 25A (1967) 274.

32) Van der Wiel, M.J., El-Sherbini, Th.M. and Vriens, L., Physica 42 (1969) 411.

33) Johansen, A., Olsen, J.S., Steenstrup, S. and Koch, J., Rad.Effects 2 (1969) 19.

34) Hart, R.R., Olson, N.T., Smith Jr., H.P., Khan, J.M., Phys.Rev. 179 (1969) 4.

35) Cairns, J.M., Holloway, D.F. and Nelson, R.S. (Proceedings European Conf.on Ion Impl., Reading 1970, Peter Peregrinus Ltd. England) and Rad.Effects to be published.

36) Roth, S., Sizmann, R., Coutelle, R., and Bell, F., Phys.Letters 32A (1970) 119.

37) Van der Weg, W.F., den Boer, J.A., Saris, F.W. and Onderdelinden, D. (Proceedings European Conf.on Ion Impl., Reading 1970, Peter Peregrinus Ltd., England).

CHAPTER II

CROSS SECTIONS FOR Ar L-SHELL AND Ne K-SHELL X-RAY EMISSION IN HEAVY ION–ATOM COLLISIONS

F. W. SARIS and D. ONDERDELINDEN

F.O.M.-Instituut voor Atoom- en Molecuulfysica, Amsterdam, Nederland

Received 16 March 1970

Synopsis

The present work deals with a series of cross-section measurements for soft X-ray emission produced by Ar^+, Ne^+, H^+ on Ar and Ne^+ on Ne. The X radiation, which is detected by a proportional counter, corresponds to vacancies in the Ar L-shell and Ne K-shell. The cross section appears several orders of magnitude smaller for proton impact than for heavy-ion bombardment, thus showing the difference in excitation mechanisms.

Mean fluorescence yields are deduced from our experimental emission cross sections and the Auger "excitation" cross sections of the innershells involved. It is observed that the fluorescence yield is influenced by the mechanism for primary vacancy creation. Finally, from the energy dependence of the cross section near threshold we determine critical internuclear distances for innershell excitation.

1. *Introduction.* Violent collisions between atomic particles are highly inelastic, as has been shown by many authors[1,2]). A precise measurement of scattering angle and energy reveals the amount of kinetic energy that is transferred into excitation and ionization of the colliding particles. Inelastic energy losses (Q values) up to 6 keV have been found[3]), more than enough to excite innershell electrons. Moreover, when the ion energy is increased high enough to force an interpenetration of inner shells, then the inelastic energy loss rises sharply and shows a triple peaked structure[4]). For homonuclear cases, such as $Ar^+ \rightarrow Ar$ and $Ne^+ \rightarrow Ne$, these results are indeed attributed to L-shell and K-shell excitations, respectively[5]). The creation of a vacancy in the atomic shells initiates two competing rearrangement processes. An Auger transition may occur which gives rise to the emission of outer-shell electrons with a well defined kinetic energy. This process is studied frequently[6]). On the other hand a radiative decay may also occur which produces emission in the soft X-ray region. This was studied for proton and helium impact on metals for many years[7,8]). Only recently soft X-ray emission during heavy ion-atom collisions became a subject of interest[3,9,10]). The present work gives a series of cross-section measurements for soft X-ray

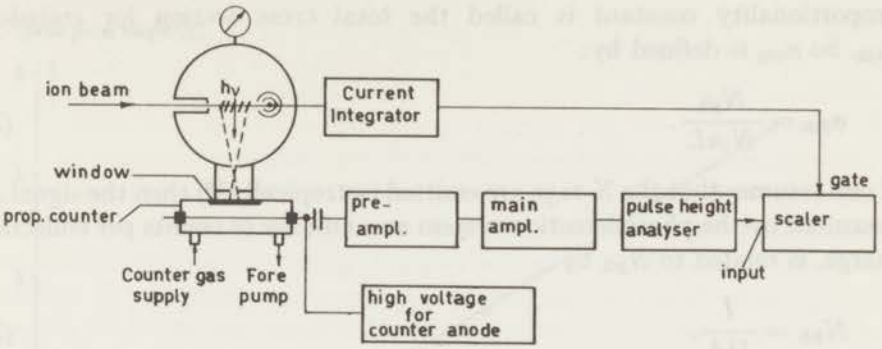

Fig. 1. A schematic diagram of the experimental setup.

emission during heavy ion–atom collisions. We first describe the apparatus and experimental method. Then the data are given on the detection system itself and on Ar L-shell and Ne K-shell X-ray emission during collisions of Ar^+, Ne^+, H^+ on Ar and Ne^+ on Ne. Finally some conclusions are drawn concerning the fluorescence yield and the inner-shell excitation mechanism.

2. *Apparatus and experimental method.* 2.1. Apparatus. The experimental setup is shown in fig. 1. A 200 keV isotope separator[11]) is used to produce the primary ion beam in the energy region above 30 keV. Below this energy the ions were extracted from a beam machine called Cesar[12]). Neutralization and excitation of the beam particles is prevented by keeping a vacuum of 10^{-6} torr in the beam line until the ions reach the scattering region. During the experiments the pressure in the target chamber is kept below 5×10^{-3} torr, which is read by a calibrated ionization gauge.

After passing through the target gas the ions are collected in a Faraday cup and measured by a current integrator. The interaction region is viewed by a proportional counter through a pair of collimators. The photodetection system consists of: a thin-window proportional counter used in flow mode, a high-voltage power supply, a preamplifier, a main amplifier, a multi- or single-channel pulse-height analyser and an electronic counter. The gate of this counter is controlled by the current integrator. The performance and efficiency of the photodetection system is described in section 2.3.

2.2. Evaluation of the emission cross section. Of common interest in many experiments is the process:

$$A^+ + B \rightarrow A^{n+} + B^{m+} + (m + n - 1)\,e + h\nu. \qquad (1)$$

We studied soft X-ray emission originating from innershell excitations that take place during such a process. The number of photons, N_{ph}, emitted is proportional to: the number of ions N_i passing through the interaction region; the density n of the target gas; the length L of the interaction region. The

proportionality constant is called the total cross section for emission σ_{em}. So σ_{em} is defined by:

$$\sigma_{em} = \frac{N_{ph}}{N_1 n L}. \tag{2}$$

If one assumes that the X rays are emitted isotropically[13]) then the signal I, measured by the photodetection system as a number of counts per collected charge, is related to N_{ph} by:

$$N_{ph} = \frac{I}{\Omega A}, \tag{3}$$

where Ω is the geometrical factor and A the efficiency factor, *i.e.* counter gas absorption and window transmission. Thus the cross-section measurement is reduced to a measurement of some fixed quantities as L, A, Ω and some variables as I, n:

$$\sigma_{em}(E_0) = \frac{I(E_0)}{N_1 A \Omega n L}. \tag{4}$$

Here the intensity of the X-ray emission is written as a function of the parameter E_0, the primary energy of the projectiles. All quantities can be determined absolutely, so the cross section is to be measured absolutely and as a function of the primary energy. The dimension of the emission cross section will be written in [cm^2].

2.3. Performance of the photodetection system. The aim of the experiments is the measurement of the absolute photon yield of argon L-shell and neon K-shell radiation. The wavelengths of these photons is about 56 Å (220 eV) and about 14.5 Å (850 eV), respectively. Proportional counters have previously been used in this soft X-ray region[14]). We employed

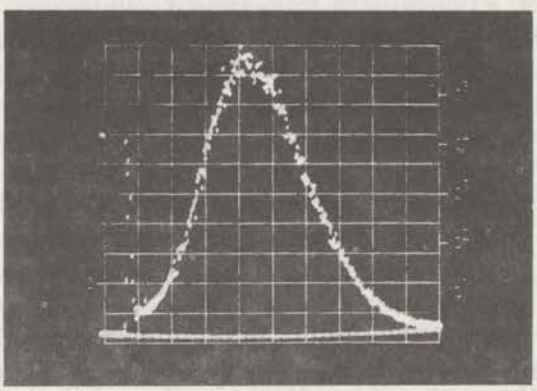

Fig. 2. Pulse-height distribution in a 400 channel pulse-height analyser for Ar L-shell X rays originating from collisions of 90 keV Ar^+ on Ar.

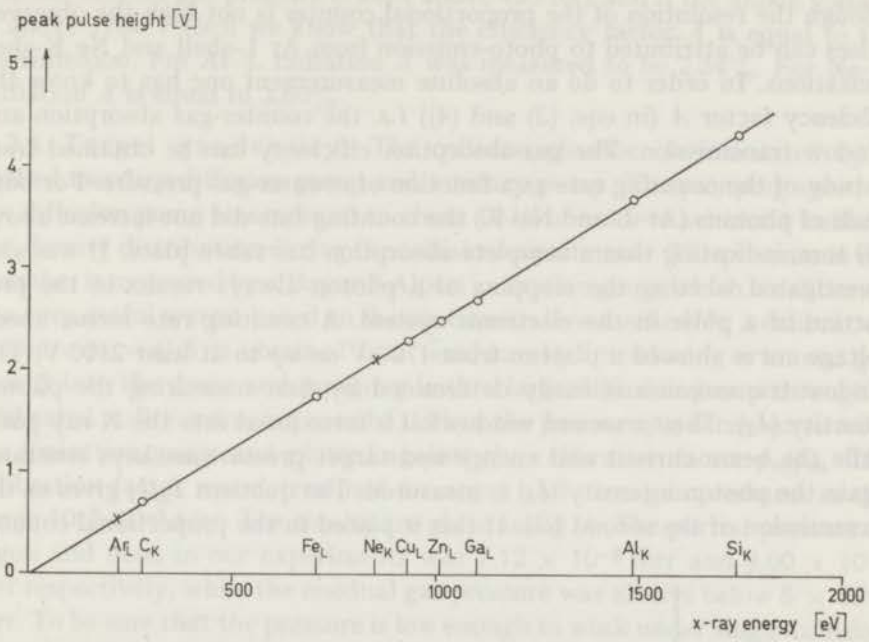

Fig. 3. Observed peak pulse heights *versus* energy of K- and L-shell X rays emitted during proton bombardment of various metal targets. The peak pulse heights observed in gas collisions as Ar^+ on Ar and Ne^+ on Ne are indicated by crosses.

a side window flow counter[15]) (commercially available from Siemens Co., Germany) 6.0 cm long and 2.52 cm inner diameter with an anode wire of 0.04 mm. The window material supplied with the counter is aluminium-coated mylar 6 μ thick. *P* 10 gas (90% argon and 10% methane) flows through the counter at atmospheric pressure. A sufficiently energetic photon which passes the window can be stopped by a photo-absorption process in the counter gas. This results in the production of photo electrons. The total charge of the electrons gives a pulse which is amplified and fed into a pulse height analyser. The pulse-height spectrum obtained while the proportional counter views collisions of 90 keV Ar^+ ions with Ar atoms is shown in fig. 2. It is seen that pulses originating from photo-emission can be easily discriminated from the noise level. In most of the experiments signals were kept below 1000 counts/s in order to avoid pile up of pulses. In order to identify the soft X rays the counter has to show a peak pulse height which is proportional to the quantum energy of the photons. This was checked by observing K- and L-shell X-ray emission from metal targets during bombardment with 90 keV protons[8]), while the anode voltage of the counter was kept at 1650 volts. The observed peak pulse heights are plotted against the X-ray energies[17]) in fig. 3. The peak pulse heights observed in the gas collision experiments $Ar^+ \rightarrow Ar$ and $Ne^+ \rightarrow Ne$ are indicated in the figure.

Though the resolution of the proportional counter is not high the observed pulses can be attributed to photo-emission from Ar L-shell and Ne K-shell excitations. In order to do an absolute measurement one has to know the efficiency factor A (in eqs. (3) and (4)) *i.e.* the counter-gas absorption and window transmission. The gas-absorption efficiency can be obtained from a study of the counting rate as a function of counter-gas pressure. For both kinds of photons (Ar–L and Ne–K) the counting rate did not increase above 450 torr, indicating that a complete absorption has taken place. It was also investigated whether the stopping of a photon always results in the production of a pulse in the electronic system. A counting rate *versus* anode voltage curve showed a plateau from 1700 V on up to at least 2100 V. The window transmission is easily determined by first measuring the photon intensity (I_1). Then a second windowfoil is introduced into the X-ray path, while the beam current and energy and target pressure are kept constant. Again the photon intensity (I_2) is measured. The quotient I_2/I_1 gives us the transmission of the second foil. If this is placed in the proportional counter

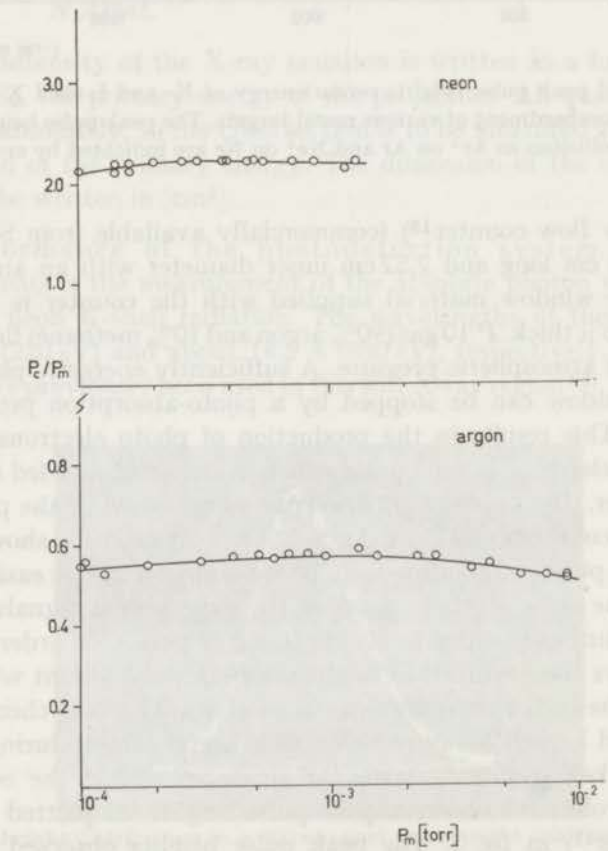

Fig. 4. The calibration of a G.E. ionization gauge for argon and neon gaspressures.

and the counter gas pressure is kept above 450 torr and if the anode voltage is above 1700 V then we know that the efficiency factor A is equal to the transmission. For Ar–L radiation A was measured to be 2.34%. For Ne–K radiation A is equal to 3.60%.

2.4. Target gas-density. The collision chamber is evacuated by a baffled mercury diffusion pump and a rotary pump. The pumping speed of the diffusion pump was reduced to about 10 l/s in order to achieve a uniform gas-density distribution during the collision experiments. The pressure in the chamber is measured by a Bayard–Alpert ionization gauge which is calibrated in a very useful system based on the continuous flow method [18]). A calibration pressure $p_c = Q/S$ is obtained in a testdome by introducing a known gas flow Q into the dome and pumping with a large diffusion pump through a calibrated orifice (pumping speed S). Then the pressure p_m is measured with the ionization gauge and plotted against the calibration factor p_c/p_m. The calibration factor was determined for argon and neon gas pressures in the range 10^{-3}–10^{-5} torr. The results are given in fig. 4. The partial pressure of argon and neon in our experiments was 1.12×10^{-3} torr and 9.00×10^{-4} torr respectively, while the residual gas pressure was always below 5×10^{-6} torr. To be sure that the pressure is low enough to work under single-collision conditions and to prevent absorptions, X-ray intensities were measured as a function of target pressure. A linear dependence of intensities on pressure was found below 5×10^{-3} torr.

At room temperature the target density n [number of atoms per cubic centimetre] is related to the pressure p [torr] by $n = 3.34 \times 10^{16}\, p$.

2.5. Experimental errors. The relative uncertainty $\Delta x/x$ is determined in percentage for all the factors of eq. (4). All relative uncertainties are added, thus giving the relative error in the cross section σ_{em}.

If the uncertainty of each geometrical reading was 0.3% then $\Delta\Omega/\Omega$ is about 4.0%. The target length in the Ar experiments was 3.50 cm and during the Ne experiments 2.60 cm with $\Delta L < 0.05$ cm making $\Delta L/L \approx 2\%$.

The beam (1 mm in diameter) is collected on the inner electrode of a cylindrical Faraday cup with two concentric electrodes to suppress the secondary electrons. The electrodes have a 2 mm diameter hole to let the beam in. Tests of bias voltage on the inner electrodes *versus* collected current showed that 60 volts were more then enough to keep all secondary electrons in the cup. Errors in current measurements can also be due to large-angle scattering or neutralization of beam particles in the target region. We checked this by measuring the current while the scattering chamber was evacuated to 5×10^{-6} torr, then the pressure was increased to 2×10^{-3} torr by flowing argon gas into the chamber. The current changes were always less than 2%. Leakage of current through the current integrator is neglected.

The error in the transmission factor A is mainly determined by the

statistics in counting rate. Due to the low transmission the total counting rate is rather low when we use two foils (see section 3.1.), thus giving a statistical uncertainty of 10%. Additional uncertainties are distortion and bowing of the foil produced by the atmospheric pressure difference accross the counter window. The estimated error in A is therefore as high as 15%.

In many cross-section experiments the error in the target gas-density measurement is in the order of 10% or more. However, the absolute accuracy obtained with the calibration system (see section 3.2.) is claimed to be better than 2% in the pressure range 10^{-3}–10^{-5} torr[18]).

The total error obtained by adding all the above uncertainties is 25%.

The statistical counting-rate error played a significant role only during σ measurements near threshold. Here the counting rate was equal to or lower than the background leading to a statistical error of 10%. So for cross sections in the order of 10^{-22} cm^2 the total error is estimated to be 35%.

3. *Results.* 3.1. Cross section for Ar L-shell X-ray emission in $Ar^+ \rightarrow Ar$ collisions. For several reasons we focused our attention to the Ar L-shell X-ray emission cross section in the homonuclear case $Ar^+ \rightarrow Ar$. For this case the innershell excitation is most frequently studied, by measur-

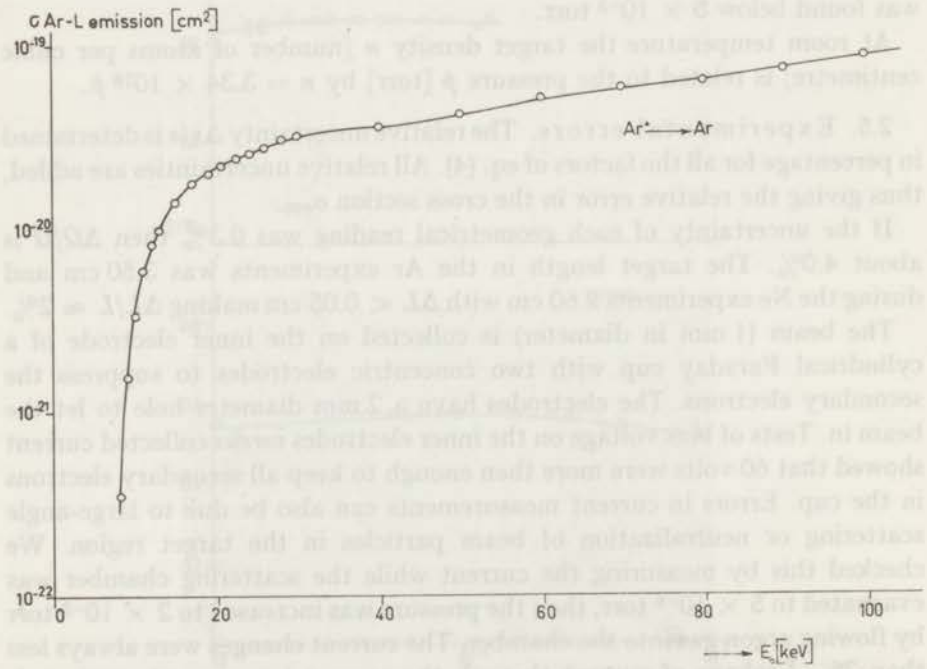

Fig. 5. Absolute cross section for Ar L-shell X-ray emission during collisions of Ar^+ on Ar *versus* primary energy of the projectile.

TABLE I

Ar L-shell X-ray yield and cross section in Ar^+ on Ar

E_0 [keV]	$I(E_0)$ [counts/N_i]	$\sigma_{em}(E_0)$ [cm^2]	E_0 [keV]	$I(E_0)$ [counts/N_i]	$\sigma_{em}(E_0)$ [cm^2]
8	47	3.5×10^{-22} a)	24	3546	2.67×10^{-20} a)
9	203	1.53×10^{-21}	25	3674	2.77
10	449	3.40	26	3759	2.83
11	775	5.85	27	3926	2.96
12	1102	8.30	28	4062	3.06
13	1373	1.04×10^{-20}	29	4137	3.12
14	1678	1.26	30	4227	3.18
15	1919	1.45			
16	2181	1.65	30	3245	3.03×10^{-20} b)
17	2415	1.82	40	3872	3.62
18	2609	1.97	50	4477	4.18
19	2762	2.08	60	5369	5.02
20	2955	2.23	70	6163	5.76
21	3153	2.37	80	6746	6.30
22	3285	2.48	90	7611	7.11
23	3426	2.58	100	8784	8.20

a) According to eq. (4) with
$\Omega = 1.02 \times 10^{-4}$, $L = 4.40$ cm,
$n = 3.12 \times 10^{13}$ cm^{-3},
$A = 2.34 \times 10^{-2}$, $N_i = 4.05 \times 10^{14}$.

b) According to eq. (4) with
$\Omega = 1.13 \times 10^{-4}$, $L = 3.50$ cm,
$n = 3.70 \times 10^{13}$ cm^{-3},
$A = 2.34 \times 10^{-2}$, $N_i = 3.12 \times 10^{14}$.

ing the inelastic energy loss[14]) and/or the Auger electrons[6]). We also needed the Ar–L emission cross section to study channeling of argon ions in a copper lattice[19]). Finally we had in view a measurement of the mean Ar–L fluoresence yield[20]). The Ar L-shell X-ray yield was obtained in the energy region from 8–100 keV. The cross section is deduced by taking into account, according to eq. (4), geometrical factors, target gas density and detection efficiency. The data are given in table I. In fig. 5 the absolute emission cross section is plotted *versus* the primary energy of the bombarding Ar ions. The cross section shows a sharp threshold at 8 keV. Between 8 keV and 15 keV it increases over two decades, then it bends over to a less steep curve which stays increasing however up to 100 keV. These features will be discussed later on.

3.2. Cross section for Ne K-shell X-ray emission in $Ne^+ \rightarrow Ne$ collisions. The sharp increase in inelastic energy loss at a certain distance of closest approach of the two colliding Ar particles was easily observed and already early attributed to an innershell excitation taking place during the collision. In parallel studies of large-angle Ne^+–Ne collisions the structure in Q values is not so pronounced[21]). Evidence for Ne K-shell excitation

TABLE II

Ne K-shell X-ray yield and cross section in Ne^+ on Ne

E_0 [keV]	$I(E_0)$ [counts/N_1]	$\sigma_{em}(E_0)$ [cm^2]	E_0 [keV]	$I(E_0$ [counts/N_1]	$\sigma_{em}(E_0)$ [cm^2]
45	6	0.70×10^{-23} a)	75	374	4.25×10^{-22}
50	38	4.30×10^{-23}	80	437	4.94
55	100	1.13×10^{-22}	85	536	6.06
60	145	1.64	90	642	7.25
65	216	2.44	95	743	8.40
70	280	3.16	100	792	8.95

a) According to eq. (4) with
$\Omega = 1.02 \times 10^{-4}$
$L = 2.60$ cm, $n = 2.97 \times 10^{13}$ cm^{-3}, $A = 3.60 \times 10^{-2}$,
$N_1 = 3.12 \times 10^{15}$.

during Ne^+–Ne collisions was found in the secondary-electron spectrum where the expected Auger peak was observed[22]). Whenever Auger electrons are detected, there is also a probability for finding corresponding photons. This probability is rather low, as can be seen in table II where emission cross sections are given for Ne K-shell X-ray emission in Ne^+–Ne collisions in the energy range 45 keV–100 keV. The excitation function is visualized in fig. 6.

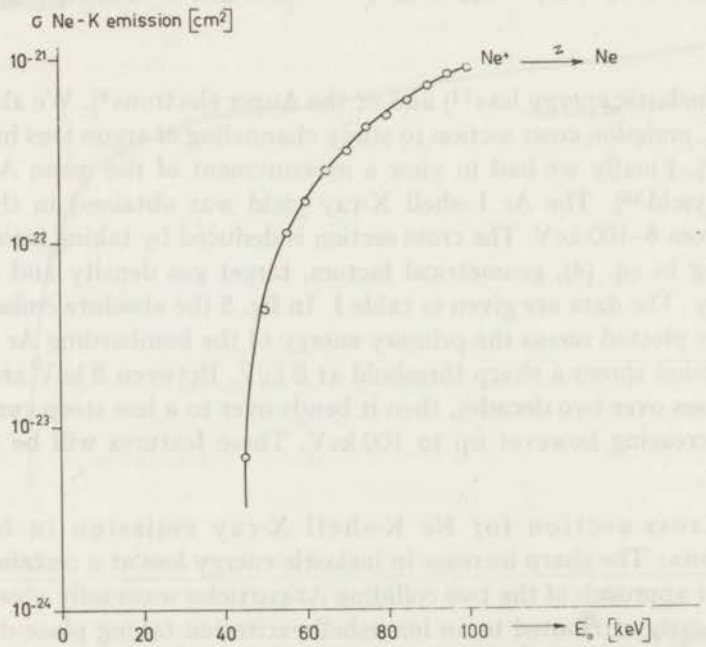

Fig. 6. Absolute cross section for Ne K-shell X-ray emission during collisions of Ne^+ on Ne *versus* primary energy of the projectile.

The first Ne K-shell X rays are detected at a primary energy of the Ne^+ beam of 45 keV. Then the cross section increases over two decades as the primary energy is doubled.

3.3. Cross section for Ar L-shell X-ray emission in $Ne^+ \rightarrow Ar$ and $H^+ \rightarrow Ar$ collisions. In a study of the asymmetric case where Ar is bombarded by Ne^+ ions[23]), the structure in inelastic energy loss, observed for the homonuclear collisions, was not obvious. After improving the energy resolution and efficiency of the detection system, one was able to study Q values and electron-energy spectra into greater detail. Recent data[24,25]) show triple peaked Q structures in a narrow range of distances of closest

TABLE III

Ar L-shell X-ray yield and cross section in Ne^+ on Ar

E_0 [keV]	$I(E_0)$ [counts/N_1]	$\sigma_{em}(E_0)$ [cm^2]	E_0 [keV]	$I(E_0)$ [counts/N_1]	$\sigma_{em}(E_0)$ [cm^2]
24	24	1.85×10^{-22} a)	60	1316	9.17×10^{-21}
25	99	7.65×10^{-22}	65	1540	1.07×10^{-20}
30	195	1.51×10^{-21}	70	1772	1.24
30	207	1.45×10^{-21} b)	75	1957	1.36
35	373	2.60	80	2167	1.51
40	539	3.76	85	2215	1.54
45	697	4.85	90	2542	1.79
50	987	6.88	95	2682	1.87
55	1132	7.90	100	2985	2.08

a) According to eq. (4) with $\Omega = 1.02 \times 10^{-4}$, $L = 4.40$ cm, $n = 3.04 \times 10^{13}$ cm^{-3}, $A = 2.34 \times 10^{-2}$, $N_1 = 4.05 \times 10^{14}$.

b) According to eq. (4) with $\Omega = 1.02 \times 10^{-4}$, $L = 2.60$ cm, $n = 3.70 \times 10^{13}$ cm^{-3}, $A = 2.34 \times 10^{-2}$, $N_1 = 6.24 \times 10^{14}$.

TABLE IV

Ar L-shell X-ray yield and cross section in H^+ on Ar

E_0 [keV]	$I(E_0)$ [counts/N_1]	$\sigma(E_0)$ [cm^2]	E_0 [keV]	$I(E_0)$ [counts/N_1]	$\sigma(E_0)$ [cm^2]
70	162	1.1×10^{-22} a)	110	323	2.3×10^{-22}
80	215	1.5	120	380	2.7
90	241	1.7	130	407	2.9
100	252	1.8			

a) According to eq. (4) with $\Omega = 1.02 \times 10^{-4}$, $L = 2.60$ cm, $n = 3.70 \times 10^{13}$ cm^{-3}, $A = 2.34 \times 10^{-2}$, $N_1 = 6.24 \times 10^{15}$.

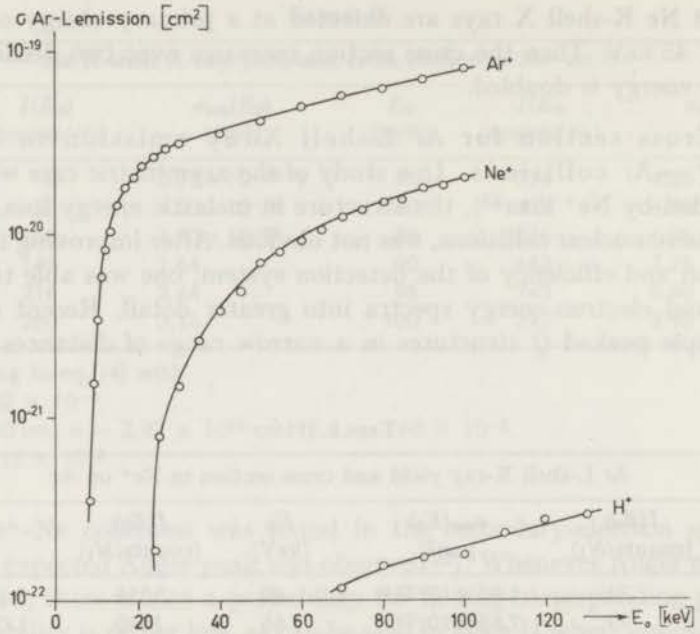

Fig. 7. Ar L-shell emission cross sections *versus* incident-ion energy for Ar^+, Ne^+ and H^+ on Ar.

approach of heteronuclear atoms. So innershell excitations also occur in asymmetric systems and we succeeded in observing Ar L-shell X-ray emission from Ne^+–Ar collisions. The photon yields have been measured in the primary energy range of 20 keV–100 keV. The yields and cross sections deduced from them are listed in table III.

Though the theory on inner-shell excitations during heavy ion–atom collisions is not well established, it is believed that the mechanism responsible for such excitations is not important for H^+ bombardment. In the molecular orbital theory the innershell electron is promoted because energy-level crossings occur as the projectile approaches the target atom close enough. Whereas innershell excitation by proton bombardment is believed to be produced by a direct scattering mechanism. In order to investigate whether the difference in excitation mechanism is shown in a difference in X-ray emission cross section, the Ar L-shell X-ray yield is measured during proton bombardment of Ar. Table IV gives the data on X-ray yield and cross section as a function of the primary proton energy in the range of 70–130 keV. In fig. 7 a comparison is made between the Ar L-shell emission cross section for Ar^+, Ne^+ and H^+ on Ar. Indeed the most striking feature is the large difference between σ_{em} for proton and heavy-ion bombardment. The cross sections for heavy ions are several orders of magnitude higher than those for

protons. The same effect has been observed for carbon K-shell excitation by Der *et al.*[10]).

3.4. Ne K-shell X-ray emission in $Ne^+ \rightarrow Ar$ collisions. We observed Ar L-shell photons from $Ar^+ \rightarrow Ar$ and $Ne^+ \rightarrow Ar$. Ne K-shell photons were observed from $Ne^+ \rightarrow Ne$, so one can wonder whether Ne K-shell photons are also emitted in $Ne^+ \rightarrow Ar$. This was investigated by analyzing the pulse-height spectrum from the proportional counter during the bombardment of Ar with 100 keV Ne^+ ions.

On the upper side of fig. 8 the pulse-height distribution is shown produced by Ar L-shell photons. The lower side shows indeed an other peak in the pulse-height spectrum which can be attributed to Ne K-shell X rays. The yield of these photons is 10^{-3} times the Ar–L yield. However, this Ne K-shell emission may originate from collisions between the Ne^+ ions and Ne atoms in the Ar gas. The partial pressure of Ne atoms due to neutralization of the Ne^+ beam in the Faraday cup is estimated to be 1×10^{-6} torr. This is 10^{-3}

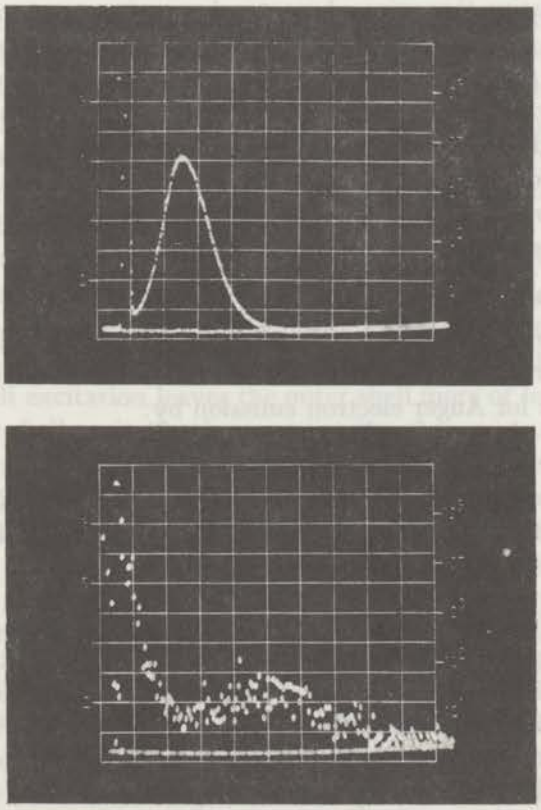

Fig. 8. Pulse-height distribution produced by photons from Ne^+ on Ar collisions. The left side shows the Ar–L X-ray peak. The right side is a magnification (400 ×) of the second half of the spectrum. The small hump is attributed to Ne–K X rays.

times the Ar gas pressure in the target chamber. The Ne–K emission cross section from $Ne^+ \rightarrow Ne$ is 5×10^{-2} times the Ar–L emission cross section. Thus Ne–K X-ray yield from $Ne^+ \rightarrow Ne$ collisions during the $Ne^+ \rightarrow Ar$ experiment will be 5×10^{-5} lower than the Ar–L emission. We measured roughly a factor of 10^{-3}, so probably the detected Ne K-shell X rays are originating from $Ne^+ \rightarrow Ar$ collisions, giving a cross section in the order of 10^{-23}[cm^2].

4. *Discussion and conclusions.* 4.1. Fluorescence yields. The creation of a vacancy in an atomic inner shell initiates two competing rearrangement processes. An Auger transition may occur which gives rise to the emission of outer-shell electrons with a well defined kinetic energy. On the other hand a radiative transition may occur which produces emission of a soft X-ray photon. Historically the fluorescence yield of an element was defined in terms of the intensity of fluorescent radiation produced when a sample of the material was exposed to a beam of energetic X rays. More recently, it has been defined in terms of the probability that a vacancy in a given shell results in a radiative transition. An extensive review on atomic fluorescence yields has been published by Fink *et al.*[20]). Besides photons and electrons, heavy charged particles can also be employed for primary vacancy production. An advantage in using ion bombardment is that the characteristic X rays produced are free of the usual bremsstrahlung background present when electron bombardment is used. The mean fluorescence yield $\bar{\omega}$ can be deduced from, $\sigma_I(E_0)$, the cross section for excitation of the innershell involved and the emission cross section $\sigma_{em}(E_0)$, because

$$\bar{\omega} = \sigma_{em}(E_0)/\sigma_I(E_0), \tag{5}$$

In many cases $\sigma_I(E_0)$ is neither theoretically nor experimentally very well known. However, the inner-shell-excitation cross section is related to $\sigma_A(E_0)$, the cross section for Auger electron emission by:

$$\sigma_I(E_0) = \sigma_A(E_0) + \sigma_{em}(E_0). \tag{6}$$

So the mean fluorescence yield can be computed from the X-ray emission cross section and the Auger electron emission cross section because substitution of eq. (6) into eq. (5) yields:

$$\bar{\omega} = \sigma_{em}(E_0)/[\sigma_A(E_0) + \sigma_{em}(E_0)]. \tag{7}$$

By way of example we use eq. (7) to calculate the fluorescence yield for the Ar L-shell and Ne K-shell. Cacak[27]) evaluated cross sections for "Auger excitation" by simply integrating the area of the fast electron peak in the secondary-electron cross section curve. However, after creation of an inner-shell vacancy it is not necessary that an Auger deexcitation process results in the emission of one and only one fast electron (see Carlson *et al.*[32]) and Bierman *et al.*[33])). So for σ_A in eq. (7) we may only use the „Auger excitation"

TABLE V

Mean fluorescence yields for the Ar L-shell and Ne K-shell deduced from σ_A and σ_{em} in symmetric collisions

E_0 [keV]	Ne^+ on Ne collision			Ar^+ on Ar collision		
	$\sigma_A(E_0)$ [cm^2]	$\sigma_{em}(E_0)$ [cm^2]	$\bar{\omega}_K$	$\sigma_A(E_0)$ [cm^2]	$\sigma_{em}(E_0)$ [cm^2]	$\bar{\omega}_L$
50	0.27×10^{-20}	4.30×10^{-23}	1.6×10^{-2}	3.30×10^{-17}	4.18×10^{-20}	1.2×10^{-3}
100	2.71×10^{-20}	8.95×10^{-22}	3.2×10^{-2}	3.87×10^{-17}	8.20×10^{-20}	2.1×10^{-3}

cross section of Cacak, if we assume that many-electron deexcitation processes are negligible. These Auger-excitation cross sections are listed in table V together with our results on the X-ray emission cross section and the fluorescence yields as calculated with eq. (7). It is very remarkable that both fluorescence yields tend to increase a factor 2 as the primary energy of the ion which creates the inner-shell vacancy is doubled. This might be caused by the excitation mechanism (see also Russek and Meli[26]). Heavy ion–atom collisions excite states which have many electrons promoted, also of the outershells. A high degree of excitation of the outer shell may diminish the chance of an Auger process and this increases the probability for a radiative decay. However, the degree of excitation is a function of the internuclear separation and thus of the primary ion energy. This may be the reason why $\bar{\omega}$ is not constant in table V. It can be checked by using a different excitation mechanism for primary vacancy creation. In section 3.3. it was stated already that the inner-shell excitation during proton bombardment is believed to be produced by a direct scattering mechanism. Probably this more gentle way of innershell excitation leaves the outer shell more or less undisturbed.

So after inner-shell excitation by a proton the chance of an Auger process will be higher and the fluorescence yield will be lower, than after excitation with a heavy ion. Rudd *et al.*[28]) obtained Ar L-Auger excitation cross sections in the same way as above for 125–300 keV proton impact on Ar. At 125 keV proton energy $\sigma_A = 6 \times 10^{-19}$ cm^2 and $\sigma_{em} = 3 \times 10^{-22}$ cm^2 (see table IV). So $\bar{\omega} = 0.5 \times 10^{-3}$ and indeed the fluorescence yield is found to be lower than obtained in the Ar^+ on Ar experiment (table V).

4.2. The excitation mechanism. Fano and Lichten have made a study of the excitation mechanism[5]). They assumed that during the collision, for example $Ar^+ \rightarrow Ar$, the ion and atom come so close that a quasi-molecule is formed which becomes a krypton atom in the limit as the internuclear separation goes to zero. Lichten[31]) calculated an energy-level diagram from energy levels of two infinitely separated argon atoms and one krypton atom. At intermediate distances energy levels of molecular orbitals are plotted. At

various points there occur crossings. If the internuclear distance becomes small enough during the collision, then at a crossing an electron may be promoted to a higher level. According to the Landau–Zener theory the chance can be evaluated for an electron to find itself in a higher energy state after separation of the colliding particles. It appears that during small impact-parameter collisions where a series of level crossings occur, excitations of inner-shell electrons become very probable.

Recently Kessel[29]) suggested to determine critical internuclear distances from the energy dependence of total X-ray emission cross sections. In the first approximation, one assumes that the inner-shell excitation is a function only of the distance of closest approach, r_0, of the two nuclei. Furthermore, it is assumed to be a very sharp function of r_0, *i.e.* no excitation for r_0 greater than a certain r_c and a constant excitation probability P for r_0 less than that value of r_c. If $p(r_c)$ is the impact parameter p at which the distance of closest approach r_0 equals r_c, then the expression for the inner-shell excitation cross section is:

$$\sigma_I = P\pi p^2(r_c). \tag{8}$$

Using a screened Coulomb interaction potential[30]) the impact parameter as a function of the distance of closest approach may be written as:

$$p(r_0) = r_0[1 - (b/r_0)\exp(-r_0/a)]^{\frac{1}{2}}; \tag{9}$$

$$b = Z_1 Z_2 e^2/E_0, \qquad a = a_0/[Z_1^{\frac{2}{3}} + Z_2^{\frac{2}{3}}]^{\frac{1}{2}},$$

Z_1 and Z_2 are the atomic numbers of the atom and ion, e is the elementary charge, E_0 is the kinetic energy of the projectile, a_0 is the Bohr radius. The energy dependence of the cross section may be found from formulae (8) and (9), thus

$$\sigma_I(E_0) = P\pi r_c^2\left[1 - \frac{Z_1 Z_2 e^2}{E_0 r_c}\exp(-r_c/a)\right]. \tag{10}$$

The X-ray emission cross section is then given by

$$\sigma_{em}(E_0) = \bar{\omega}\sigma_I(E_0). \tag{11}$$

The threshold behaviour of $\sigma_{em}(E_0)$ is sufficient to determine the value of r_c, for the type of emission whose total cross section is measured. $\bar{\omega}$ can be used as a parameter which is determined by the best fit between the curves of the calculated excitation cross section and measured emission cross section. In the case of Ar^+ on Ar many crossings of the $4f\sigma$ orbital with higher levels occur as the internuclear separation becomes smaller than 0.3×10^{-8} Å. So according to Lichten[31]) the probability for Ar L-shell ionization is estimated to be one at such close collisions (see also ref. 22). Since there are two argon atoms involved two L-shell electrons will be promoted and P in eq. (10)

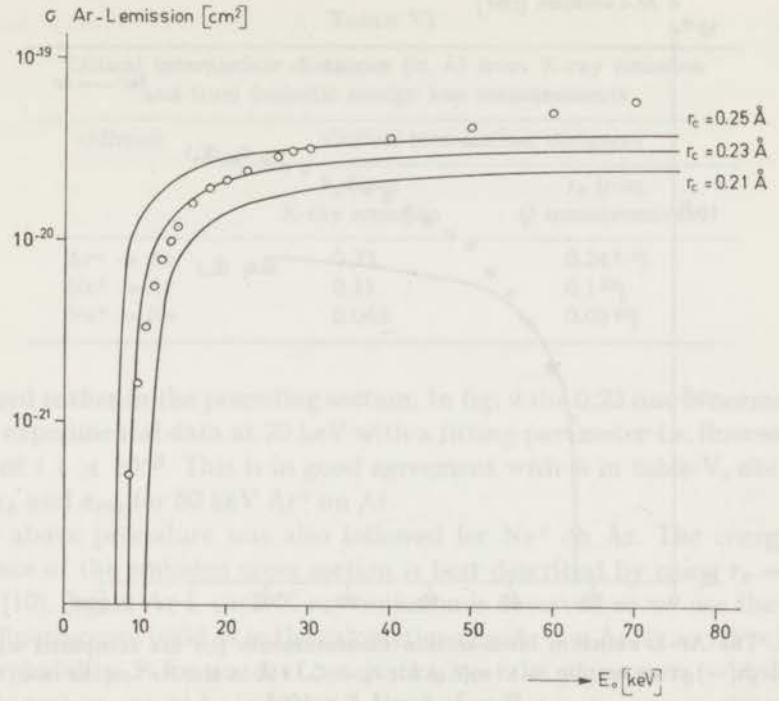

Fig. 9. The Ar–L emission cross-section measurements (○) are compared with the calculated (—) cross section $\bar{\omega} \times \sigma_I(E_0)$ for different r_c: 0.25 Å, 0.23 Å, 0.21 Å in the Ar^+ on Ar case; $P = 2$; $\bar{\omega} = 1.1 \times 10^{-3}$.

will be 2 for $r_0 \leq r_c$. The energy dependence of the cross section is calculated using eq. (10) for different values of r_c: 0.25 Å, 0.23 Å, 0.21 Å. The calculated $\sigma_I(E_0)$ is compared with the measured $\sigma_{em}(E_0)$ in fig. 9. The threshold behaviour of the $\sigma_{em}(E_0)$ is best described by $r_c = 0.23$ Å, which means that in this model 0.23 Å is the critical internuclear separation of the two Ar particles at which the Ar L-shell excitation takes place. A difference of 10% in r_c is more than enough to give a discrepancy in cross sections near threshold of an order of magnitude.

At higher energies the calculated cross sections are always lower than the measured data which remain increasing with E_0. This may be caused by several effects. Firstly, the assumption may not be true that the excitation is only a function of r_0. Probably the relative velocity of the colliding particles plays a role also. Secondly, additional L-shell vacancies may be created at smaller r_0 values. Photon emission from these excited states is added because the resolution of the proportional counter is not good enough to resolve photons from different subshells. The third reason might be that the fluorescence yield is changing as the primary energy of the projectiles is increased. The significance of this effect was

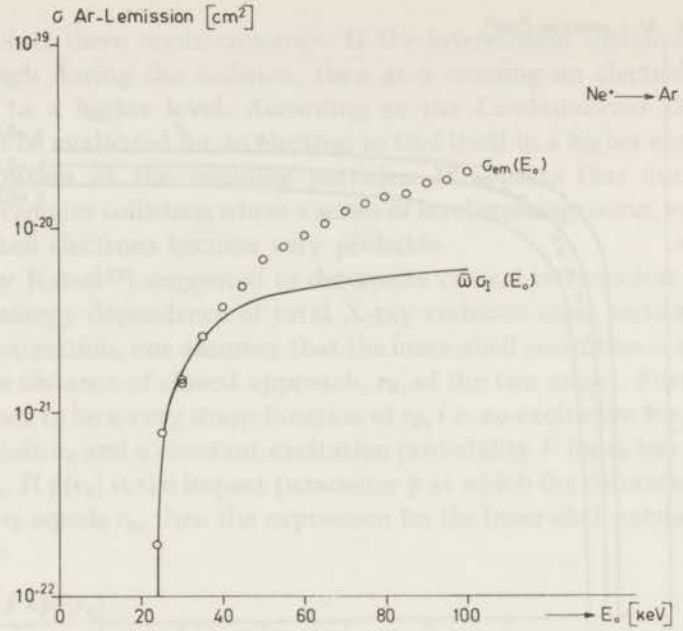

Fig. 10. The Ar–L emission cross-section measurements (○) are compared with the calculated (—) cross section $\bar{\omega} \times \sigma_I(E_0)$ for $r_c = 0.11$ Å in the Ne^+ on Ar case; $P = 2$; $\bar{\omega} = 1.1 \times 10^{-3}$.

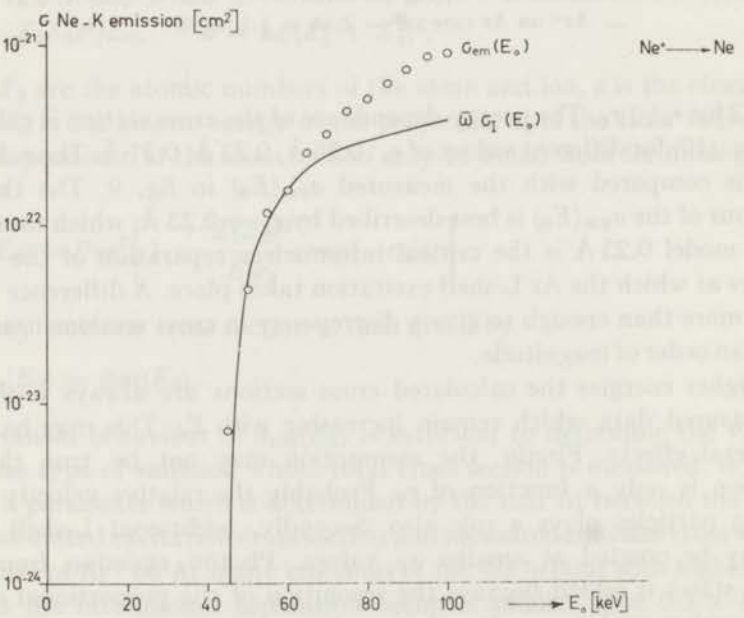

Fig. 11. The Ne–K emission cross-section measurements (○) are compared with the calculated ( ) cross section $\bar{\omega} \times \sigma_I(E_0)$ for $r_c = 0.048$ Å in the Ne^+ on Ne case $P = 0.06$; $\bar{\omega} = 1.6 \times 10^{-2}$.

TABLE VI

Critical internuclear distances (in Å) from X-ray emission and from inelastic energy loss measurements

collision	Critical internuclear distances	
	r_c from X-ray emission	r_c from Q measurements
$Ar^+ \rightarrow Ar$	0.23	0.24[1,2])
$Ne^+ \rightarrow Ar$	0.11	0.1[25])
$Ne^+ \rightarrow Ne$	0.048	0.05[22])

discussed earlier in the preceding section. In fig. 9 the 0.23 line is normalized to the experimental data at 20 keV with a fitting parameter *i.e.* fluorescence yield, of 1.1×10^{-3}. This is in good agreement with $\bar{\omega}$ in table V, obtained from σ_A and σ_{em} for 50 keV Ar^+ on Ar.

The above procedure was also followed for Ne^+ on Ar. The energy dependence of the emission cross section is best described by using $r_c = 0.11$ in eq. (10). Again Ar L-shell X-ray emission is observed so we use the same mean fluorescence yield as in the calculations for Ar^+ on Ar, $\bar{\omega} = 1.1 \times 10^{-3}$. The probability P for an Ar–L excitation to take place as $r_0 = r_c$ in the Ne^+–Ar system, might be less than 2. But recently it is shown experimentally that two Ar L-shell electrons are excited in Ne^+–Ar[25]) and other heteronuclear collisions[24]). The curve in fig. 10 is obtained with $P = 2$. The same model can also be applied to $Ne^+ \rightarrow Ne$ in order to determine the critical internuclear distance for Ne K-shell excitation. From the energy-level diagram of Lichten it is clear that promotion of K electrons can occur only at very small internuclear separations. But here it is hard to tell what the excitation probability should be. We first determined that $r_c = 0.048$ Å approaches the energy dependence of $\sigma_{em}(E_0)$ best (see fig. 11). Here the fitting parameter is equal to $\bar{\omega} \times P = 1.0 \times 10^{-3}$. The Ne K-shell fluorescence yield is known to be 1.6×10^{-2} (see table V). So in this model the excitation probability for the Ne K-shell at $r_c = 0.048$ should be $P = 0.06$.

Finally we compare the critical internuclear distance, r_c, with data from various authors on r_0 values at which a structure in inelastic energy loss is observed (see table VI).

Acknowledgements. The authors would like to thank Professor J. Kistemaker, Professor A. Russek and Dr. F. J. de Heer for their stimulating interest during the course of the research, and Dr. Q. Kessel for enlightening communications. In addition many invaluable discussions with Dr. W. F. v. d. Weg and Drs. D. Bierman are gratefully acknowledged. The authors are very much indebted to S. Doorn and H. Roukens for their help in carrying out the experiments as well as those people of the Space Research

Laboratory in Utrecht who helped in putting up the photodetection system.

This work is part of the research program of the Stichting voor Fundamenteel Onderzoek der Materie (Foundation for Fundamental Research on Matter) and was made possible by financial support from the Nederlandse Organisatie voor Zuiver-Wetenschappelijk Onderzoek (Netherlands Organization for the Advancement of Pure Research.

REFERENCES

1) Fedorenko, N. V., Uspekhi fiz. Nauk **68** (1959) 481; see Soviet Physics-Uspekhi (English Transl.) **2** (1959) 526;
Afrosimov, V. V., Gordeev, Yu. S., Panov, M. N. and Fedorenko, N. V., Zh. tekh. Fiz. **34** (1964) 1613, 1624, 1637; see Soviet Physics-Technical Physics **9** (1965) 1248, 1256, 1265. (English Transl.)
2) Morgan, G. H. and Everhart, E., Phys. Rev. **128** (1962) 667.
3) Kessel, Q. C., Rose, P. H. and Grodzins, L., Phys. Rev. Letters **22** (1969) 1031.
4) Kessel, Q. C., Russek, A. and Everhart, E., Phys. Rev. Letters **14** (1965) 484.
5) Fano, U. and Lichten, W., Phys. Rev. Letters **14** (1965) 627.
6) Rudd, M. E., Phys. Rev. Letters **13** (1964) 503.
7) Merzbacker, E. and Lewis, H. W., Handbuch der Physik (edited by S. Flügge, Springer–Verlag, Berlin) **34** (1958) 166.
8) Khan, J. M., Potter, D. L. and Worley, R. D., Phys. Rev. **139** (1965) 1735.
9) Saris, F. W., Weg, W. F. v. d. and Kistemaker, J., Phys. Letters **26A** (1968) 592.
10) Der, R. C., Kavanagh, F. M., Khan, J. M., Curry, B. P. and Fortner, R. J. Phys. Rev. Letters **21** (1968) 1731.
11) Snoek, C., thesis, Amsterdam (1966).
12. Wolterbeek Muller, L. and de Heer, F. J., Physica, to be published.
13) Schaaffs, W., Handbuch der Physik (edited by S. Flügge, Springer-Verlag, Berlin) **30** (1957) 1.
14) Samson, J. A., Vacuum Ultraviolet Technology, John Wiley and Sons, Inc. (New York, 1967).
15) Caruso, A. J. and Neupert, W. M., Appl. Optics **4** (1965) 247.
16) Korff, S. A., Electron and Nuclear Counters, Van Nostrand (Princeton, 1949).
17) Bearden, J. A., Rev. mod. Phys. **39** (1967) 78.
18) Bannenberg, J. and Tip, A., Proceeding of the 4th Int. Vacuum Congress, Manchester (1968).
19) Saris, F. W., Weg, W. F. v. d. and Onderdelinden, D., Rad. Effects **1** (1969) 137.
20) Fink, R. W., Jopson, R. C., Mark, H., Swift, C. D., Rev. mod. Phys. **38** (1966) 513.
21) Afrosimov, V. V., Gordeev, Yu. S., Panov, M. N. and Fedorenko, N.V., Zh. tekh. Fiz. **36** (1966) 123; see Soviet Physics–Technical Physics **11** (1966) 89.
22) Kessel, Q. C., Mc. Caughey, M. P. and Everhart, E., Phys. Rev. **153** (1967) 57; Phys. Rev. Letters **6** (1966) 1189.
23) Kessel, Q. C., Proceedings of VICPEAC, Leningrad (1967).
(edited by L. Branscomb, J.I.L.A. Boulder, 1968) p. 92.
24) Fastrup, B. and Hermann, G., Phys. Rev. Letters **23** (1969) 157.
25) Afrosimov, V. V., Gordeev, Yu. S., Polyansky, A. M., and Shergin, A. P., Proceedings of VIICPEAC, Boston 1969 (edited by I. Amdur, MIT Press, Cambridge 1969) p. 744.
26) Russek, A. and Meli, J., Physica **46** (1970) 222.

27) Cacak, R. C., thesis, Lincoln, Nebraska (1969).
28) Volz, D. J. and Rudd, M. E., Proceedings of VIICPEAC, Boston 1969 (edited by I. Amdur, MIT Press, Cambridge 1969) p. 410.
29) Kessel, Q. C., Bull, A. P. S. **14** (1969) 946 and private communication.
30) Everhart, E., Stone, G. and Carbone, R. J., Phys. Rev. **99** (1955) 1287.
31) Lichten, W., Phys. Rev. **164** (1967) 131.
32) Carlson, Th. A., Hunt, W. E. and Krause, M. O., Phys. Rev. **151** (1966) 41.
33) Bierman, D. J., Weg, W. F. v. d., Snoek, C. and Onderdelinden, D., Physica **46** (1970) 244.

CHAPTER III

CROSS SECTIONS FOR Ar L-SHELL X-RAY EMISSION IN COLLISIONS OF He^+, C^+, N^+, O^+, Al^+, Cl^+, Ti^+, Fe^+, Cu^+ ON Ar

F. W. SARIS

F.O.M.-Instituut voor Atoom- en Molecuulfysica, Amsterdam, Nederland

Received 12 November 1970

Synopsis

Ar L-shell X-ray emission is observed in collisions of He^+, C^+, N^+, O^+, Al^+, Cl^+, Ti^+, Fe^+, Cu^+ on Ar thus proving that innershell vacancies are produced during these heavy-ion–atom collisions. The cross sections for Ar L-shell X-ray emission show to be strongly dependent on the atomic number of the projectile. The data are discussed in the framework of the Fano–Lichten model for innershell excitations. Critical internuclear distances for innershell excitation are deduced from the threshold of the cross sections and compared with data from other investigators. These critical internuclear distances present a characteristic oscillation, which is correlated to the Z dependence of the geometrical sizes of the innershells involved.

1. *Introduction.* Only recently soft X-ray emission resulting from heavy-ion–atom collisions became a subject of interest. Inelastic energy losses have been studied extensively in the homonuclear cases, $Ar^+ \rightarrow Ar$ and $Ne^+ \rightarrow Ne$[1]). At small distances of closest approach one observes structures in the inelastic energy-loss distributions that are attributed to L-shell and K-shell excitation, respectively. The innershell vacancies decay preferentially via an Auger process resulting in the ejection of fast electrons. However, a radiative decay may also occur thus producing photon emission in the soft X-ray region. The observation of structure in the inelastic energy-loss distribution at small distances of closest approach is an indication that innershell excitation takes place during heavy ion–atom collisions. However, the proof of the innershell vacancy production is in the subsequent emission of Auger electrons or characteristic X rays. The use of thin-window proportional counters to detect soft X rays made it relatively easy to investigate total cross sections for characteristic X-ray emission in heavy-ion–atom collisions. Such cross sections have been determined from solid targets[2,3,4]) and gaseous targets as well[5]). Supplementary to the inelastic energy-loss and Auger-electron emission data, we determined cross sections for Ar L-shell X-ray emission in $Ar^+ \rightarrow Ar$, $Ne^+ \rightarrow Ar$, $H^+ \rightarrow Ar$, and Ne K-shell X-ray emission in $Ne^+ \rightarrow Ne$.

In the present work various heteronuclear collisions on Ar are investigated. Total cross sections for Ar L-shell X-ray emission are determined in He^+, C^+, N^+, O^+, Al^+, Cl^+, Ti^+, Fe^+, Cu^+ on Ar. These cross sections show to be strongly dependent on the atomic number of the projectile. The data will be discussed in the framework of the Fano–Lichten model for innershell excitation. Critical internuclear distances for innershell excitation are deduced from the threshold of the cross sections and compared with data from other investigators.

2. *Apparatus and experimental method.* The experimental setup has been described in detail earlier[5]). A 200 keV isotope separator ($mE \leq 4 \times 10^6$ [(proton mass) eV]) is used to produce the primary ion beam in the energy region above 30 keV. The accelerator is equipped with a sputter ion source[6]) to make available ions of both solids and gases. Neutralization and excitation of the beam particles is prevented by keeping a vacuum of 10^{-6} torr in the beam line until the ions reach the scattering region. During the experiments the differentially pumped target chamber is filled with argon gas with a pressure below 5×10^{-3} torr to be sure that single-collision conditions are fulfilled. After passing through the target gas the ions are collected in a Faraday cup and measured by a current integrator. The proton detection system consists of a thin-window proportional counter used in flow mode, a high-voltage power supply, a pre-amplifier, a main amplifier, a pulse height analyser and an electronic counter. The gate of the counter is controlled by the current integrator.

The emission cross section is defined by:

$$\sigma_{em} = N_{ph}/N_i nL, \tag{1}$$

N_{ph} is the number of photons emitted per N_i, the number of ions passing through the interaction length L, n is the density of the target gas. If one assumes that the characteristic X rays are emitted isotropically[7]), then the signal I, measured by the photo detection system as a number of counts per collected charge, is related to N_{ph} by

$$N_{ph} = I/\Omega A, \tag{2}$$

where Ω is the geometrical factor and A the efficiency factor *i.e.* counter gas absorption and window transmission. Thus the cross section is:

$$\sigma_{em} = I/N_i A \Omega nL. \tag{3}$$

During all measurements N_i, A, Ω, n and L were fixed, $N_i = 3.12 \times 10^{14}$, $A = 2.34 \times 10^{-2}$, $n = 3.70 \times 10^{13}$ cm^{-3}, $L = 2.60$ cm. The X-ray yield I was measured as a function of energy from 30 keV up to the highest ion energy available from the accelerator. Since all quantities can be determined absolutely, the cross section is also determined absolutely. In the cases of

TABLE I

Ar L-shell X-ray emission cross sections in $Z^+ \rightarrow Ar$

E_0 [keV]	$He^+ \rightarrow Ar$ $\sigma[cm^2]$	$C^+ \rightarrow Ar$ $\sigma[cm^2]$	$N^+ \rightarrow Ar$ $\sigma[cm^2]$	$O^+ \rightarrow Ar$ $\sigma[cm^2]$	$Al^+ \rightarrow Ar$ $\sigma[cm^2]$	$Cl^+ \rightarrow Ar$ $\sigma[cm^2]$	$Ti^+ \rightarrow Ar$ $\sigma[cm^2]$	$Fe^+ \rightarrow Ar$ $\sigma[cm^2]$	$Cu^+ \rightarrow Ar$ $\sigma[cm^2]$
30		0.53×10^{-20}	0.64×10^{-20}	0.51×10^{-20}		1.22×10^{-20}	2.22×10^{-20}	0.10×10^{-20}	
35		0.83	0.83	0.80		1.35	3.00	0.28	
40		0.88	0.89	1.01		1.70	4.25	0.46	
45		1.18	1.04	1.09		2.45	5.30	0.74	0.63×10^{-21}
50		1.26	1.36	1.41		2.16	5.70	1.20	1.51
55		1.41	1.43	1.73	0.09×10^{-20}	2.29	6.55	1.70	3.02
60		1.49	1.68	2.02	2.13	2.79	8.21	2.24	4.42
65		1.68	1.82	2.56	2.66	2.94	8.62	2.95	4.60
70		2.02	2.10	2.77	3.72	3.46	1.10×10^{-19}	3.53	
75		2.10	2.34	3.14	4.26	3.68	1.18	4.00	
80		2.38	2.24	3.35	5.59	4.31	1.30		
85		2.38	2.48	3.64	5.85	5.03	1.25		
90	2.1×10^{-22}	2.69	2.85	4.00	7.45	5.50			
95		2.92	2.93	4.18	9.05	6.06			
100	2.9	3.30	3.20	4.42		6.80			
110	3.5								
120	4.8								
130	5.1								

metal-ion bombardment also relative measurements were done as a control. The Ar L-shell X-ray yield during the metal-ion bombardment could easily be compared with Ar^+ bombardment, because argon was used in the sputter ion source as support gas. The experimental accuracy with which the quantities in formula (3) can be measured is discussed in ref. 5. The total error is mostly below 25%.

3. *Results.* By means of eq. (3) the emission cross sections are deduced from the X-ray yields and listed in table I. In the cases of C^+ on Ar and Cl^+ on Ar the data may be erroneous, for the resolution of the proportional counter is not good enough to discriminate between pulses from Ar–L photons ($\approx$ 250 eV) and C–K photons ($\approx$ 280 eV) or Cl–L photons ($\approx$ 200 eV). So in these two cases the table should read X-ray emission rather than Ar L-shell X-ray emission.

In fig. 1 the cross sections are plotted *versus* relative energy of the two colliding particles. Here the earlier data for Ar^+, Ne^+ and H^+ on Ar are added. The cross sections for H^+ and He^+ ions show to be several orders of magnitude lower than those for heavy-ion bombardment. This is attributed to a Coulomb type of excitation mechanism in the cases of H^+ and He^+[3,4,5,12] which will not be discussed in this paper. For most of the cross sections the lowest primary energy was low enough to determine the threshold. Above this threshold the excitation functions increase sharply with energy.

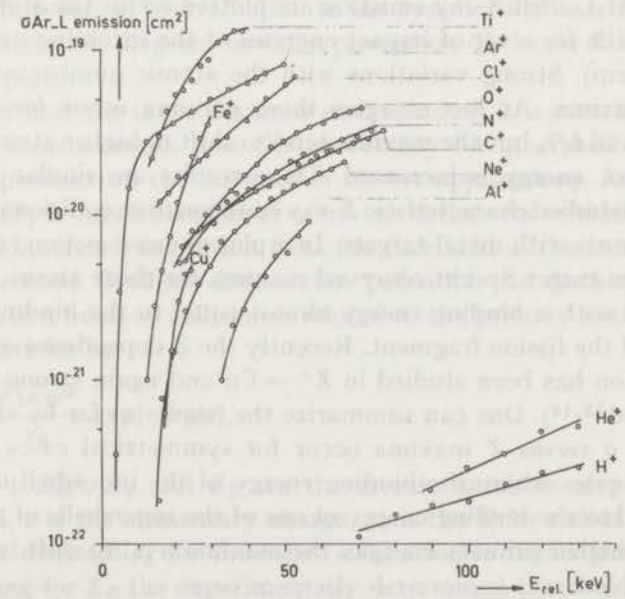

Fig. 1. Cross sections for Ar L-shell X-ray emission in $Z^+ \rightarrow$ Ar *versus* incident-ion energy E_{rel} (in centre of mass system).

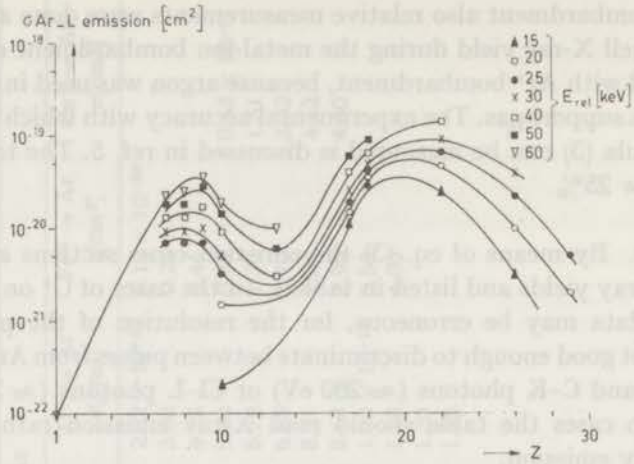

Fig. 2. Cross sections for Ar L-shell X-ray emission in $Z^+ \rightarrow$ Ar *versus* the atomic number of the projectile. The data are plotted for a set of impact energies (in c.m. system).

4. *Discussion.* The aim of this work was to investigate the influence of the projectile on the cross section for Ar L-shell X-ray emission in heavy-ion–atom collisions. From fig. 1 it is obvious that the cross sections for the symmetrical case $Ar^+ \rightarrow$ Ar is higher than for all the other ions except one. It is very illustrative to plot the data differently, like fig. 2. Here the cross sections for Ar L-shell X-ray emission are plotted *versus* the atomic number of the projectile for a set of impact energies of the incoming ion (in centre of mass system). Strong variations with the atomic number are observed with two maxima. At low energies these maxima occur for the atomic numbers 18 and 6/7, but the maxima tend to shift to higher atomic numbers as the impact energy is increased. These results are similar to those of Specht[2]) who studied characteristic X-ray emission from collisions of energetic fission fragments with metal targets. In a plot of cross section *versus* atomic number of the target Specht observed maxima for those atoms which have an innershell with a binding energy almost equal to the binding energy of the L-shell of the fission fragment. Recently the Z dependence of Cu L-shell X-ray emission has been studied in $Z^+ \rightarrow$ Cu and again strong oscillations were observed[13,14]). One can summarize the results so far by stating that: in a plot of σ *versus* Z maxima occur for symmetrical cases and quasi-symmetrical cases where the binding energy of the innershell under study is about equal to the binding energy of one of the innershells of the collision partners. At higher primary energies the maxima tend to shift to a higher Z number.

Fano and Lichten[8]) have proposed a theoretical model for the innershell excitation in heavy-ion–atom collisions. They assumed that during the

collision of Ar^+ on Ar the ion and atom come so close that a quasi-molecule is formed. From a correlation diagram for molecular orbitals of a symmetric diatomic system, Lichten[15]) constructed energy level diagrams of molecular orbitals of the Ar–Ar and Ne–Ne systems. At various internuclear distances there occur crossings of energy levels. If the distance of closest approach during the collision becomes small enough, then at a crossing an electron may be promoted to a higher energy level. In the Ar–Ar case the numerous crossings of the $4f\sigma$ molecular orbital with higher orbitals may account for the promotion of Ar L-shell electrons. If one wants to apply the Fano–Lichten model to the excitation of Ar L-shell electrons in heteronuclear collisions on argon, then one should first construct correlation diagrams for molecular orbitals of these asymmetrical diatomic systems. Herzberg[16]) described the building-up principles for such correlation diagrams. We have to consider that the lowest σ orbital in the nearly united atoms can only go over into the lowest σ orbital in the near atoms. The second-lowest σ orbital goes into the second lowest, and so on; π, δ ... orbitals behave correspondingly. Two different σ (or π, δ ...) orbitals cannot intersect if the internuclear distance is changed except when other quantum numbers than the angular momentum are taken into account. Thus the correlation diagram for molecular orbitals of asymmetrical systems do not show such crossings as observed in the symmetrical case. Correlation diagrams do not indicate more than the qualitative behaviour of the energies of the orbitals with variation of the internuclear distance. No detailed calculations giving exact curves are available. However, in contradiction to the symmetrical case it is not clear from the correlation diagram how the promotion of the Ar L-shell electron might take place.

No matter how the inner electrons are promoted it is seen from inelastic energy-loss measurements that the probability for innershell excitation is strongly dependent on the distance of closest approach r_0. Assuming that the probability is only a function of r_0 one can deduce the critical internuclear distance for innershell excitation from the threshold of the cross section[17]). Using a screened Coulomb interaction potential the distance of closest approach r_0 in a head-on collision is related to the primary energy E_0 of the colliding particles by

$$E_0 = \frac{Z_1 Z_2 e^2}{r_0} \exp(-r_0/a), \tag{4}$$

$a = a_0/(Z_1^{\frac{2}{3}} + Z_2^{\frac{2}{3}})^{\frac{1}{2}}$, Z_1 and Z_2 are the atomic numbers of projectile and target atom, e is the elementary charge, a_0 is the Bohr radius. The critical internuclear distance r_c for innershell excitation is found from eq. (4) by simply taking for E_0 the experimentally determined threshold of the cross section. In fig. 3 the r_c values for Ar L-shell excitation in collisions of Z^+ on Ar are plotted *versus* the atomic number Z. A comparison is made with

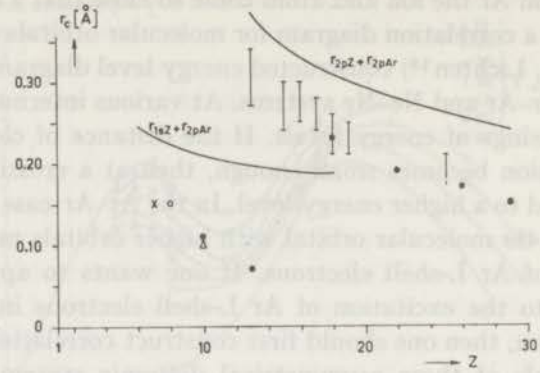

Fig. 3. Critical internuclear distances for Ar L-shell excitations in collisions of Z^+ on Ar plotted *versus* Z;
from our X-ray measurements ●, from structure in inelastic energy-loss distributions: I "active r_0 regions"[18]), △ from ref. 19, ○ from Bingham[20]) who observed an "active region" from 0.11 to 0.20 Å, × from ref. 21. The solid lines show the sum of the radii[22]) of maximum charge density for the wave functions of 2p electrons of argon and 2p or 1s electrons of the projectile.

data on the "active r_0 region" where structure in the inelastic energy-loss distribution is observed by other investigators[18–21]). Going from Cu ($Z = 29$) to Ar ($Z = 18$) the critical internuclear distance increases steadily, which is continued until $Z = 13$. For $Z = 25$, 19, 18, 17, 16, 15 and 13 the "active r_0 regions" are shown as observed by Fastrup and Hermann[18]), who attribute the structure in the inelastic energy-loss distribution found for $13 \leq Z < 18$ to L-shell excitation not of argon but of the projectile. For Al^+ on Ar we observe an interesting case: at large internuclear distances ($0.27\ \text{Å} \leq r_c \leq 0.34\ \text{Å}$) Al L-shell excitation occurs whereas for a much smaller value of r_c ($= 0.07$ Å) the Ar L-shell photon is observed.

The Al L-shell vacancy is produced at internuclear distances small enough to cause an interpenetration of L-shells of projectile and target atom. In order to procedure an Ar L-shell vacancy we have to force the collision partners to internuclear distances for which the Al K-shell and Ar L-shell overlap. In fig. 3 the r_c values increase again going from $Z = 13$ to 8/7 where we can only indicate a lower limit to r_c but inelastic energy-loss measurements give here $r_c \simeq 0.15$ Å[20,21]). In order to illustrate the geometrical effect of the shell sizes one can simply add the radii of maximum charge density for the wave functions of 2p electrons of argon and 2p or 1s electrons of the projectile. This is shown in fig. 3 by the solid lines for $r_{2pZ} + r_{2pAr}$ and $r_{1sZ} + r_{2pAr}$. The data strongly suggest that the excitation of the Ar L-shell happens for $Z \leq 18$ via interaction of the L-shells of projectile and target atom, whereas for $6 \leq Z < 18$ the excitation is dominated by a K–L overlap. Apparently a considerable overlap of interacting shells is required

before excitation takes place. Although the geometrical effect sheds some light on the excitation mechanism it does not elucidate the shift of the maxima observed in fig. 2.

Finally it should be emphasized that we have neglected the influence of the collision velocity on the excitation probability.

Acknowledgments. The author would like to thank Professor J. Kistemaker, Professor J. Los and Dr. F. J. de Heer for their stimulating interest during the course of the research and for their comments and discussions. In addition S. Doorn and H. Roukens are thanked for their help in carrying out the experiments.

This work is part of the research program of the Stichting voor Fundamenteel Onderzoek der Materie (Foundation for Fundamental Research on Matter) and was made possible by financial support from the Nederlandse Organisatie voor Zuiver-Wetenschappelijk Onderzoek (Netherlands Organization for the Advancement of Pure Research).

REFERENCES

1) See the review article of Kessel, Q. C., in Case Studies in Atomic Collision Physics I, edited by E. W. McDaniel and M. R. McDowell, North-Holland Publ. Comp. (Amsterdam, 1969) p. 401.
2) Specht, H. J., Z. Phys. **185** (1965) 303.
3) Der, R. C., Kavanagh, F. M., Khan, J. M., Curry, B. P. and Fortner, R. J., Phys. Rev. Letters **21** (1968) 1731.
4) Brandt, W. and Laubert, R., Phys. Rev. Letters **24** (1970) 1037.
5) Saris, F. W. and Onderdelinden, D., Physica **49** (1970) 441.
6) Hill, K. J. and Nelson, R. S., Nuclear Instrum. and Methods **38** (1965) 15.
7) Schaaffs, W., Handbuch der Physik, edited by S. Flügge, Springer Verlag (Berlin) **30** (1957) 1.
8) Fano, U. and Lichten, W., Phys. Rev. Letters **14** (1965) 627.
9) Rudd, M. E., Jorgensen Jr., T. and Volz, D. J., Phys. Rev. **151** (1966) 28.
Cacak, R. K., Kessel, Q. C. and Rudd, M. E., Phys. Rev. A (to be published,.
10) Volz, D. J. and Rudd, M. E., Phys. Rev. A (to be published).
11) Snoek, C., Geballe, R., Weg, W. F. van der, Rol, P. K. and Bierman, D. J., Physica **31** (1965) 1553.
12) Stein, H. J., Lutz, H. D., Mokler, P. H., Sistemich, K. and Armbruster, P., Phys. Rev. Letters **24** (1970) 701.
13) Cairns, J. A., Holloway, D. F. and Nelson, R. S., Atomic Collision Phenomena in Solids, edited by Palmer, D. W., Thompson, M. W., Townsend, P. D., North-Holland Publ. Comp. (Amsterdam, 1970).
14) Khan, J., private communication.
15) Lichten, W., Phys. Rev. **164** (1967) 131.
16) Herzberg, G., Molecular Spectra and Molecular Structure I., Spectra of Diatomic Molecules, D. van Nostrand, inc. (Princeton N. J., 1950).

17) Kessel, Q. C., Bull. A.P.S. **14** (1969) 946.
18) Fastrup, B. and Hermann, G., Phys. Rev. Letters **23** (1969) 157.
19) Afrosimov, V. V., Gordeev, Yu. S., Polyansky, A. M. and Shergin, A. P., Proceedings of VIICPEAC, Boston 1969, edited by I. Amdur, MIT-Press (Cambridge, 1969) p. 744.
20) Bingham, F. W., Phys. Rev. **182** (1969) 180.
21) Knystautas, E. J., Kessel, Q. C., DelBoca, R. and Hayden, H. C., Phys. Rev. **A1** (1970) 825.
22) Slater, J. C., Quantum Theory of Atomic Structure I, McGraw-Hill Book Comp. (New York, 1960) p. 210.

CHAPTER IV

CHARACTERISTIC X-RAY PRODUCTION BY Ar^+ AND Ne^+ IRRADIATION OF MONOCRYSTALLINE COPPER

1. *Introduction.* It is known that inelastic processes occur during the slowing down of fast particles in solids. This is manifested in numerous ways, one of which is the emission of characteristic X-rays. In a violent collision inside the solid an innershell of the collision partners may be ionized. A radiative decay process results in the production of a characteristic X-ray photon that can escape into the vacuum. In studying the X-ray emission during ion bombardment of solids one can investigate physical processes occurring in biparticle collisions, see refs. 1,2,3,4, 5). On the other hand the generation of characteristic X-rays has become a tool in studying ion implantation in solids by making use of the channeling phenomenon [6,7]. By channeling is meant that the trajectory of a particle may have a certain stability near the centre of an open direction in a single crystalline lattice. In a channel the projectile is traveling in a region of low atomic density. This reduces the probability of all those physical effects that require a close collision between incident particle and target atom. Therefore, whenever an energe-

tic ion beam enters a monocrystalline target within the appropriate critical angle to a low index direction, a minimum is observed in Rutherford scattering, nuclear reactions, sputtering, secondary electron emission and also in characteristic X-ray production.

In the present work the irradiation of 30 - 100 keV Ar^+ and Ne^+ ions into single crystalline copper is investigated by means of the X-ray yield. Ar L-shell, Ne K-shell and Cu L-shell X-rays are detected utilizing a proportional counter. The characteristic X-ray yields are measured as a function of the angle of incidence of the primary ion beam with respect to the [110], and [100] channeling directions. As reported earlier we find a drastic deviation from the above pattern of behaviour [8]. It will be shown that the knowledge of the X-ray emission cross sections for the biparticle collisions involved enables us to understand the experimental data qualitatively. The difference between the X-ray emission

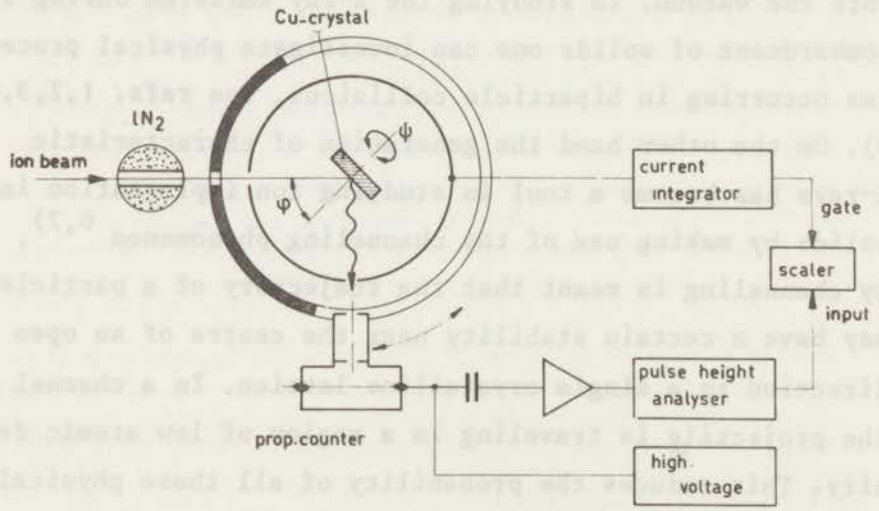

Fig. 1. Schematic diagram of the experimental setup.

probability during atomic collisions in solids and in gases will also be discussed.

2. *Apparatus and experimental method.* A schematic diagram of the experimental setup is shown in fig. 1. The ion beam with an energy between 30 and 100 keV enters a scattering chamber through collimating slits and hits the target. The beam divergence is 0.7° and a typical current density is 2 $\mu A/mm^2$. We used very high doses of primary ions $\sim 10^{17}$ cm^{-2}. In order to suppress secondary electron emission the target is situated inside a Faraday cage thus providing accurate current measurements. The target manipulator provides two independent rotations: the front surface of the crystal can be turned over an angle ϕ with respect to the beam direction, whereas the crystal can be rotated over an angle ψ about the surface normal. We used 99.999% pure Cu single crystals with surfaces having (100) or (110) orientation. The crystals are mechanically polished first and then electropolished before mounting in the targetholder. The pressure in the target chamber is 10^{-6} torr. A liquid nitrogen trap is put into the beamline to prevent carbon layers to be built up on the target surface. Moreover the sputtering rate of 30 - 100 keV Ar^+ and Ne^+ on Cu is high enough to maintain a clean surface (degree of covering less than 5%) [9]. Characteristic X-rays are observed with a side window proportional counter at an angle of observation of 90° with respect to the ion beam.

The performance of the photodetection system is described extensively in ref. 10). During Ar^+ bombardment of copper

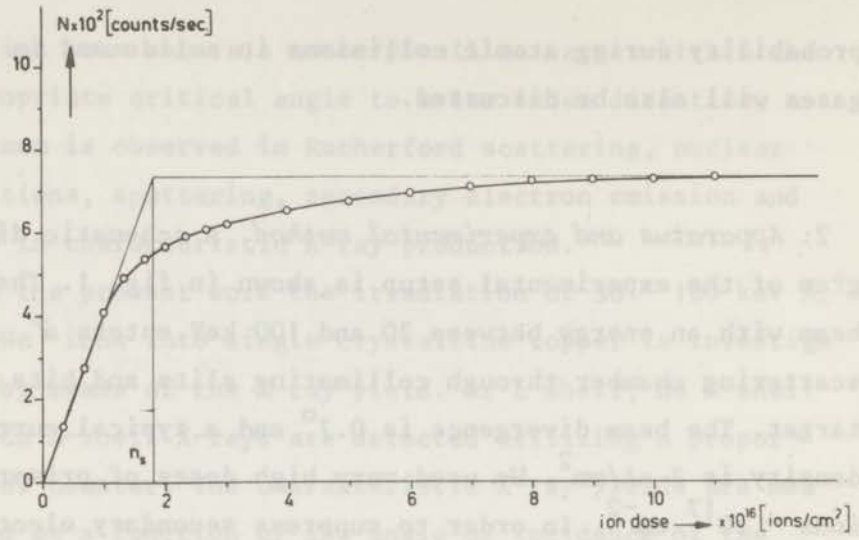

Fig. 2. A typical collection curve. The number of counts per second produced by Ar-L photons is plotted versus the dose of 30 keV Ar^+ ions incident on a copper (100) surface in a nonchanneling direction at $\phi = 45^\circ$.

we are able to detect Ar L-shell X-rays (~ 250 eV) and Cu L-shell X-rays (~ 390 eV) separately. In the case of Ne^+ bombardment only one peak is observed in the pulse height spectrum, for the resolution of the proportional counter is not good enough to distinguish between pulses from Cu L-shell X-rays and Ne K-shell X-rays (~ 850 eV).

In the experiments the noble gas ions are accumulated in the copper target. This results in the production of X-rays arising from collisions of the projectile with previously implanted projectile atoms, which can only be avoided by using extremely low ion doses. However the sputtering action of the ion beam was necessary to keep the target surface free from contamination. The accumulation effect is clearly illustrated in fig. 2. The Ar L-shell X-ray yield is plotted versus the dose of 30 keV Ar^+ ions. After sufficiently long bombardment time saturation of the target is reached. This means that for

every collected ion one gas atom must leave the target. This subject will be discussed later on, it is important to note here that in this paper the X-ray yield is called the number of counts per ion after saturation of the target has been reached.

3. *Directional effects in the X-ray production.* Fig. 3 shows the angular dependence of the X-ray production by Ar^+ ions of 90 and 35 keV. In fig. 3a the (100) copper surface is bombarded under an angle $\phi = 45^o$, whereas it is rotated about the normal over an angle ψ with respect to the [110] direction. To our surprise 35 keV Ar^+ ions generated a maximum in Ar-L X-ray yield when the beam was

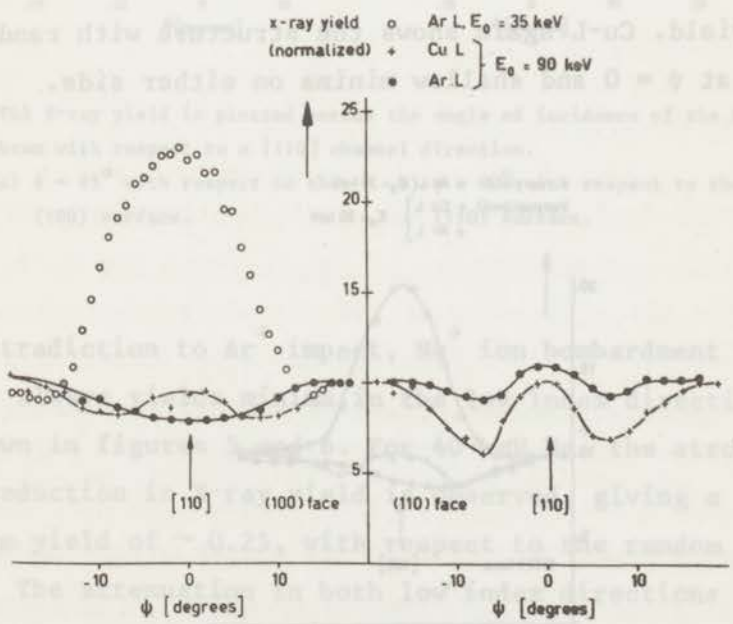

Fig. 3. The X-ray yield is plotted versus the angle of incidence of the Ar^+ ion beam with respect to a [110] channel direction.
a) $\phi = 45^o$ with respect to the (100) surface.
b) $\phi = 60^o$ with respect to the (110) surface.

directed into the [110] channel. The yield in the aligned case is 2.3 times the random yield. In the case of 90 keV Ar^+ ions a shallow minimum is observed. During 90 keV Ar^+ ion bombardment we are able to detect also Cu-L X-rays, showing a yield which is equal to the random yield in the aligned case ($\psi = 0^o$) with shallow minima on either side. A similar structure is observed for the Ar-L and Cu-L X-ray yield in fig. 3b. Here a (110) copper surface is bombarded under an angle $\phi = 60^o$, and again rotated over an angle ψ with respect to the [110] channel direction. As seen in fig. 4 also a maximum in Ar L-shell X-ray yield occurs when a 35 keV Ar^+ ion beam is directed into the [100] channel; $\phi = 45^o$ with respect to the (110) surface. For 90 keV a shallow minimum is observed in the Ar-L yield. Cu-L again shows the structure with random yield at $\psi = 0$ and shallow minima on either side.

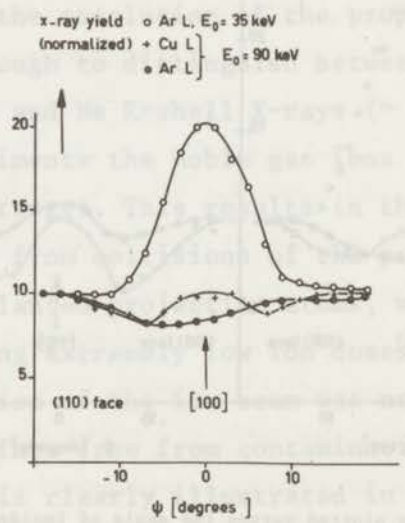

Fig. 4. The X-ray yield is plotted versus the angle of incidence of the Ar^+ ion beam with respect to a [100] channel direction, $\phi = 45^o$ with respect to the (110) surface.

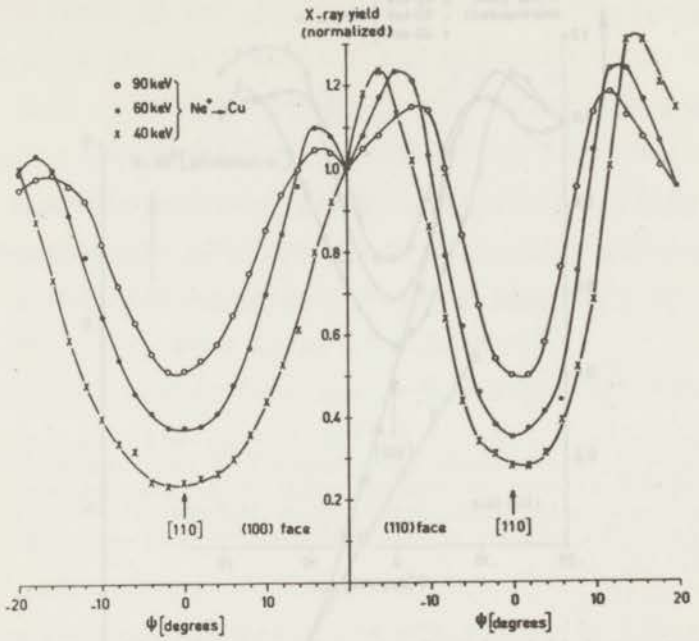

Fig. 5. The X-ray yield is plotted versus the angle of incidence of the Ne^+ ion beam with respect to a [110] channel direction.
a) $\phi = 45^\circ$ with respect to the (100) surface.
b) $\phi = 60^\circ$ with respect to the (110) surface.

In contradiction to Ar^+ impact, Ne^+ ion bombardment of copper always yields minima in the low index directions, as shown in figures 5 and 6. For 40 keV Ne^+ the strongest reduction in X-ray yield is observed, giving a minimum yield of ~ 0.25, with respect to the random yield. The attenuation in both low index directions decreases as the impact energy is increased.

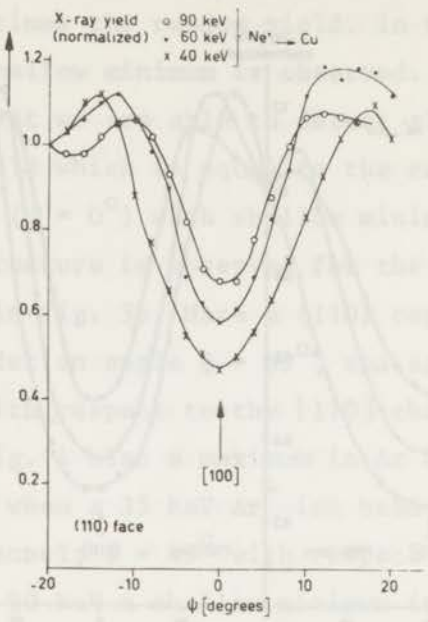

Fig. 6. The X-ray yield is plotted versus the angle of incidence of the Ne^+ ion beam with respect to a [100] channel direction, $\phi = 45^\circ$ to the (110) surface.

4. *Total Ar-L X-ray yields.* So far we have only reported relative measurements. If one corrects the X-ray yield for the efficiency of the photodetection system and the geometrical factor then the absolute "thick target yield" is known. The detection efficiency is taken from ref. 10) (= 2.34%), the geometrical correction factor is 1.78×10^{-5}. The Ar L-shell X-ray production was determined as a function of the impact energy of Ar^+ ions, bombarding a Cu (100) surface at an angle of incidence of 45° in a nonchanneling direction and in the [110] direction. Fig. 7 again shows that at low energies the intensity in the aligned case is higher than in the random case and this situation is reversed for high energies.

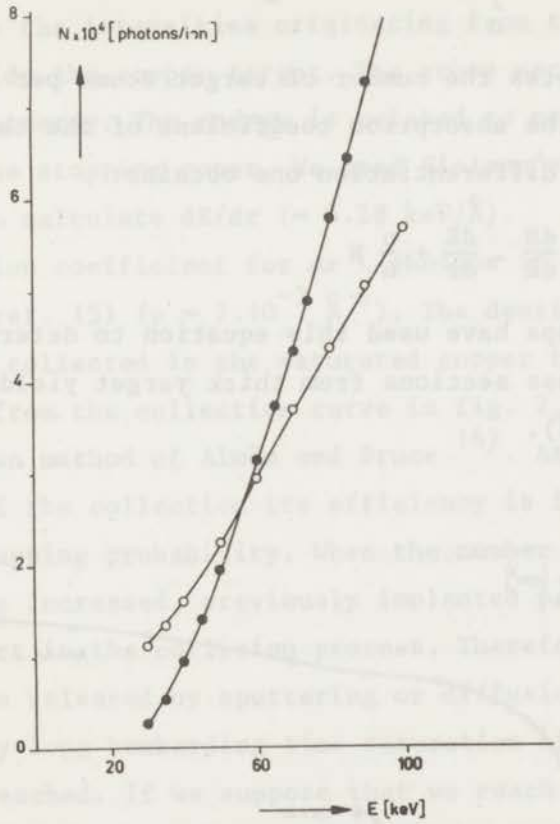

Fig. 7. The total Ar-L "thick target yield" plotted versus the impact energy of the Ar^+ ion beam incident under 45° with a copper (100) surface, in a nonchanneling direction ● ; and in the [110] direction ○ .

With the target making an angle of 45° with both the ion beam and the observed X-ray, a photon traverses about the same thickness of the target material as the ion which produces it. If an ion with an energy E(r), corresponding to a residual projected range r, has a cross section $\sigma_x[E(r)]$ for the production of the characteristic

X-rays, then ions of total range R_o will produce an X-ray yield $N(R_o)$:

$$N(R_o) = n \int_o^{R_o} e^{-\mu(R_o - r)} \sigma_x[E(r)]\, dr \qquad (1)$$

where n denotes the number of target atoms per unit volume, and μ the absorption coefficient of the target, (see ref. 1). By differentiation one obtains:

$$\sigma_x = \frac{1}{n} \frac{dN}{dE} \cdot \frac{dE}{dr} + \frac{\mu}{n} N \qquad (2)$$

Several groups have used this equation to determine X-ray emission cross sections from thick yarget yields, ref. 1, 3, 4, 11, 12).

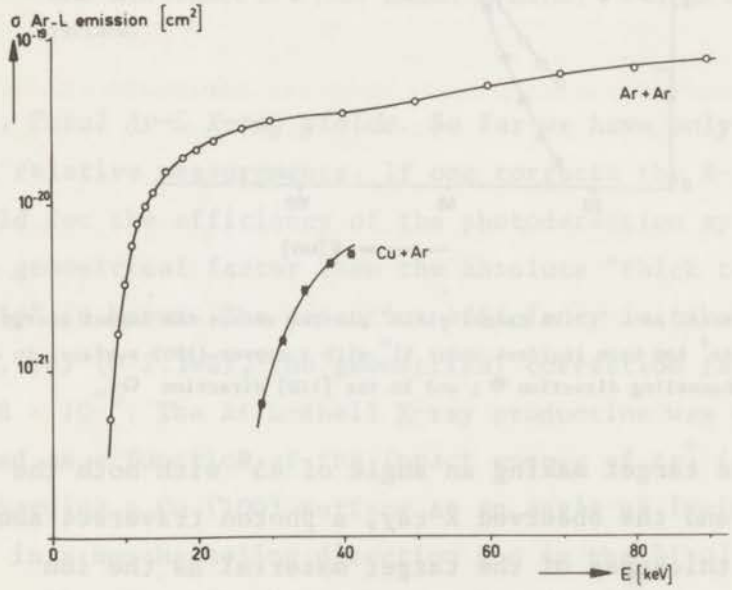

Fig. 8. Cross sections for Ar-L X-ray emission plotted versus impact energy of the Ar^+ ion. The Ar + Ar data are taken from ref. 10), the Ar + Cu data are from ref. 13).

The total yield plotted in fig. 7 originates not only from collisions of Ar^+ on Cu but also from Ar^+ on Ar. Since we know the Ar L-shell X-ray emission cross section [13] for both collisions (see fig. 8), we can use eq. 1 to calculate the intensities originating from these collisions inside the copper target. The cross section is a function of energy. The energy is related to penetration depth via the stopping power. We used Nielsen's stopping power [14] to calculate dE/dr (= 0.28 keV/Å).
The absorption coefficient for Ar L photons in copper was taken from ref. 15) ($\mu = 7.10^{-3}$ Å^{-1}). The density of argon atoms collected in the saturated copper target can be deduced from the collection curve in fig. 2, following the wellknown method of Almèn and Bruce [16]. At the beginning of the collection its efficiency is identical with the trapping probability. When the number of trapped particles is increased, previously implanted particles can take part in the collision process. Therefore trapped atoms can be released by sputtering or diffusion. After sufficiently long bombarding time saturation of the target is reached. If we suppose that we reach the saturation value along the straight line through the origin, which represents the efficiency then we can construct the saturation value n_s for the ion dose (see fig. 2). If the concentration of injected atoms is taken to be constant to a depth corresponding to the mean range where it rapidly decreases, then the saturation dose should be devided by this range to give the number density of implanted argon. At 35 keV Ar^+ on Cu the density n becomes equal to 1.2×10^{-2} Å^{-3}. Assuming that the density varies in-

versely proportional to the sputtering yield [22], we can use the same argon density throughout the energy region from 30 - 90 keV because S changes only slightly [17]. Substitution of the above quantities in eq. 1 and integration yields the number of Ar-L photons resulting from

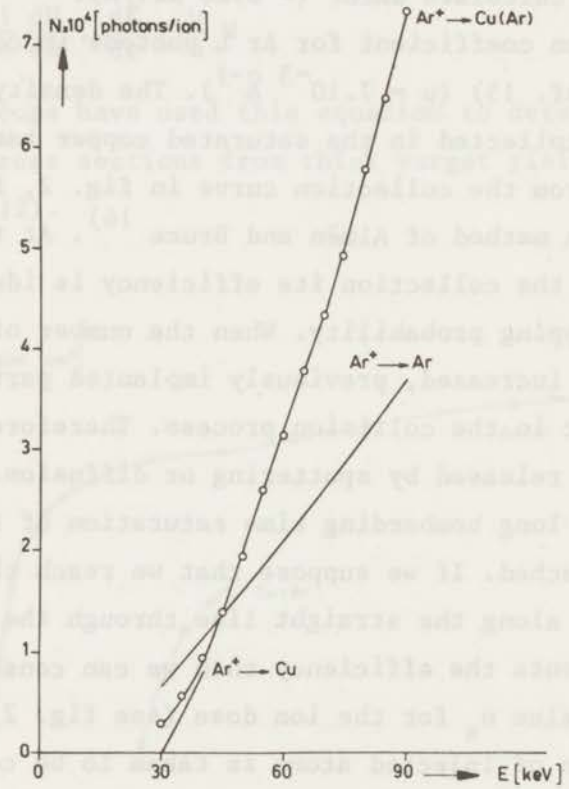

Fig. 9. The total Ar-L "thick target yield" plotted versus the impact energy of the Ar^+ ion beam incident under 45^o with a copper (100) surface in a nonchanneling direction. The $Ar^+ \rightarrow Cu(Ar)$ line shows the experimental data (see fig. 7). The solid lines show the calculated yields from A $Ar^+ \rightarrow Ar$ collisions inside the copper target, and from $Ar^+ \rightarrow Cu$ collisions.

collisions of Ar^+ on Ar inside the copper target, see fig. 9. Using eq. 1 we can also calculate the Ar-L X-ray yield resulting from Ar^+ on Cu. The cross section is known between 25 and 40 keV, see fig. 8; $n = 8.65 \times 10^{-2}$ Å^{-3}; $\mu = 7.10^{-3}$ Å^{-1}; $dE/dr = 0.28$ keV Å. The calculated thick target yield from Ar^+ - Cu (25 - 40 keV) collisions is also shown in fig. 9.

5. *Discussions.*

5.1. X-ray emission from violent atomic collisions in solids and in gases. In fig. 9 a discrepancy is seen between the calculated and observed Ar-L X-ray yield. Below 50 keV the calculated yield is higher than the observed total yield. One can wonder how much the calculations in the forgoing paragraph are to be trusted. A big uncertainty is caused by the accumulation effect. The number of argon atoms collected in saturation can be estimated, but the depth distribution is very uncertain. The assumed constant concentration overestimates the X-ray intensity from collisions of the projectile with implanted projectiles. Moreover the photon absorption coefficient is only valid for pure copper. The layer through which the photons travel is a compound of Ar and Cu, which will have a different and probably higher absorption coefficient for Ar-L photons than in pure copper. With the stopping power used one calculates the residual energy of a projectile which traveled through the crystal over a certain range. However, this range is not equal to the projected range for which eq. 1 was derived. The correction on the total pathlength in order

to find the projected range is large: (see for instance ref. [7,25]) $R_o/r \simeq (1 + M_2/3M_1)^{-1} \simeq 2/3$. In connection to this it should also be emphasized that the effective target stopping power is increased by gas occlusion and radiation damage which will be discussed later.

Perhaps the largest discrepancy between the calculated and observed yield is caused by the cross section. During the measurements of cross sections for X-ray emission in atomic collisions in gases care has been taken to work under single collision conditions with a well defined beam of singly charged argon atoms [10]. For several reasons it is rather doubtful whether these cross sections can be applied to calculate the X-ray yield from atomic collisions in a solid target.

1 - The degree of excitation or ionization of the outer shells of the collision partner affects the probability for excitation of an innershell electron. For example, with the symmetric neon collisions Everhart's [23] group showed that in Ne^{++}-Ne the excitation cross section for the Ne K-shell was twice that of the Ne^{+}-Ne case. Similar results are reported by Ogurtsov [24] for Ar^{++} on Ar.
It has been known for years that the mean ionization of energetic heavy ions which traverse solids reaches a value greater than one [18]. The mean charge state is determined by the competition between capture and loss of electrons, which is a function of the velocity of the particle. So the excitation probability for the L-shell of an argon ion penetrating a copper target is different from biparticle collisions in

gases because the mean charge state will be higher than one and will change as the particle is slowing down.

2 - The creation of a vacancy in an atomic innershell initiates two competing rearrangement processes. An Auger transition may occur which gives rise to the emission of outershell electrons. On the other hand a radiative decay may occur. The fluorescence yield is defined as the probability that a vacancy in a given shell results in a radiative transition. This probability is strongly dependent on the impact energy and kind of ion that created the innershell vacancy, see ref. 10). So for the above reasons the fluorescence yield is unknown inside the solid.

The consequence of the above arguments is that the thick target yield is determined by rather complex factors, which are too much simplified by eq. 1. It is to be expected that the use of this equation yields extremely large errors.

5.2. The angular dependence of Ar-L X-ray production. From the theoretical work of Lindhard [19] it is known that if the angle of incidence of a beam is smaller than a critical angle ψ_c with respect to a low index direction then a large fraction of the beam becomes channeled. For heavy ions at keV energies:

$$\psi_c = (3\, Z_1 Z_2\, e^2 a^2 \,/\, 4\pi\varepsilon_o d^3 E)^{\frac{1}{2}} \qquad (3)$$

$a = 0.8853\, a_o/(Z_1^{2/3} + Z_2^{2/3})^{\frac{1}{2}}$, Z_1 and Z_2 are the atomic number of projectile and target atom, a_o is the Bohr radius, e is the elementary charge, ε_o is the dielectric

constant, d is the atomic spacing along the aligned row, E is the impact energy, ref. 9). An important aspect of the channeling phenomenon is the fact that a channeled particle cannot approach closer to a lattice site than a certain r_{min}. This minimum distance is given by

$$r_{min} = \psi_c \, d \qquad (4)$$

Using eq. (3) and (4) we calculated r_{min} for 35 keV and 90 keV Ar^+ incident on single crystalline copper in the [110] and [100] directions.

E_o	r_{min}	
	[110]	[100]
35 keV	0.382 Å	0.418 Å
90 keV	0.304 Å	0.335 Å

The critical internuclear distance r_c for Ar L-shell excitation has been determined in collisions of Ar^+ + Ar and Cu^+ + Ar [13]. In the symmetrical Ar case r_c = 0.23 Å, in the Ar + Cu case r_c = 0.15 Å. Hence, a strong attenuation in the Ar-L yield is expected as the beam becomes channeled in the copper lattice. A necessary condition for channeling is a perfect lattice structure. In fact, the channeling technique is used to study damage in solids. If a beam of particles is aligned into a channeling direction then it is split into a channeled and a random component. In principle the interaction yield of the total beam is determined by the magnitude of the random component. However a channeled particle may interact with a lattice imperfection, i.e. it is de-

channeled. Then it is added to the random component and an increase in interaction yield is observed. In the channeling technique the increase is used as a measure for the rate of imperfection inside the solid. Recently it has been shown that the above is in fact an over-simplified model. Due to flux peaking of a well channeled beam its interaction yield with lattice imperfections (for instance interstitials) is not equivalent with the random beam [20].

In our work, during 35 keV Ar^+ bombardment of copper a marked increase in Ar-L X-ray yield is observed as the beam is injected into a low index direction, see figures 5 and 6. This must be attributed to two effects.

a) A large amount of disorder is created by the incident ions. The disorder causes dechanneling which enlarges drastically the random component of the beam. The range distribution of channeled beams in semiconductors was studied extensively in recent years. It has been shown that total doses above 10^{13} ions/cm^2 produce a drastic reduction of the channeled fraction of the beam [7]. In metals this sensitivity to ion dose is not so high. It was shown by Eriksson [21] that in tungsten a total dose of more than 3.10^{15} K^+ ions/cm^2 is necessary to cause a change in range distribution. Unfortunately the concentration profiles of Ar implanted in copper have not been studied sofar. However, in our experiments we used dose levels in excess of 10^{16} ions/cm^2, so it is rather likely that lattice disorder will cause dechanneling of the aligned beam, see also ref. 6 and 22).

b) During bombardment in a low index direction the accumulation of projectile atoms is more effective than in a nonchanneling direction. The variation of the saturation dose with the orientation of the ion beam with respect to a single crystalline target was shown to be approximately inversely proportional to the sputtering ratio [16,22]. Therefore in the aligned case in our experiments the dechanneled particles travel through a region with larger argon density, thus giving rise to a higher Ar-L X-ray yield.

At 35 keV the above effect is very important because at these relatively low energies the Ar-L X-rays are predominantly generated by Ar + Ar collisions inside the copper lattice. In fig. 8 it is seen that at 35 keV the cross section in the Ar + Cu collision is just above threshold, whereas in the Ar + Ar case 35 keV is approximately four times the threshold energy. At 90 keV the cross section in Ar + Cu will be high enough to increase the influence of this collision on the X-ray production. At high energies also the penetration depth of the argon ions is increased such that the absorption of Ar-L photons becomes more important. For instance 75% of the photons generated by dechanneled particles at a depth of 200 Å is absorbed. This is illustrated by the shallow minima observed for the Ar-L yield as the 90 keV Ar^+ beam is impinging under 45° with the surface normal, fig. 3a and fig. 4. If the angle of incidence is more oblique then again a maximum appears, fig. 3b.

5.3. The angular dependence of Ne-K and Cu-L X-ray production. The minimum distance of a neon ion to the

channel walls in the copper lattice can again be calculated with eq. 3 and eq. 4. At 90 keV r_{min} to the [110] string is 0.262 Å and to the [100] string 0.286 Å. The critical internuclear distance r_c for Ne K-shell excitation has been determined for the Ne^+ + Ne collision [10], r_c = 0.05 Å. For the asymmetrical case Ne^+ + Cu the r_c is not known. However, it is expected that for Ne K-shell or Cu L-shell excitation a considerable overlap is necessary of the innershells involved [13]. This means that r_c < 0.14 Å and again a strong attenuation of the X-ray yield is expected as the beam becomes channeled, because $r_{min} > r_c$. Indeed a reduction in yield is observed as the neon beam is aligned in the [100] and [$\bar{1}$00] directions in the copper lattice. So one is inclined to infer that the collection and dechanneling of projectiles do not play such an important role during neon irradiation as they do in the argon case. An important aspect is that 40 keV is about the threshold for Ne K-shell X-ray production in Ne^+ + Ne collisions [10]. A neon ion penetrating the first atomic layers of the solid target loses too much energy, also when it is channeled, to cause innershell excitation in Ne + Ne collisions in deeper layers. This is also the reason why the X-ray minima in figs. 5 and 6 are shallower as the impact energy is increased to 90 keV. Furthermore there is a difference in the trapping of argon and neon in copper. The bigger argon atom causes more strain in the copper lattice than the neon atom does, see for instance ref. 22). In our experimental results this is perhaps illustrated by the angular dependence of the Cu-L X-ray yield during argon bombardment (figs. 3 and 4).

Apparently the 90 keV Ar^+ ion is readily dechanneled by the dilated lattice surrounding the trapped atoms.

6. *Conclusion.* In principle characteristic X-ray production can be used to study channeling of Ar^+ and Ne^+ into a copper single crystal. The critical internuclear distances for innershell excitation during Ar + Cu and Ne + Cu collisions are smaller than the minimum distance of a channeled particle to a string. However, care should be taken to avoid accumulation of a large number of projectile atoms within the target. At large dose levels the radiation damage causes dechanneling and X-rays will be generated by collisions between projectile and previously implanted projectile atoms. The sensitivity to these effects depends strongly on the kind of ion and on its impact energy also regarding the threshold of the X-ray excitation function. The above effects must explain qualitatively the observed anomalies in the X-ray yield. The complexity of the problem as yet makes it impossible to gather quantitative information from the experimental data. Finally, it should be emphasized that the probability for X-ray production in heavy ion-atom collisions in gases can differ drastically from collisions in solids.

REFERENCES

1) Merzbacher, E. and Lewis, H.W., Handbuch der Physik (edited by S. Flügge, Springer-Verlag, Berlin) 34 (1958) 166.
2) Specht, H.J., Z.Physik 185 (1965) 301.
3) Der, R.C., Kavanagh, F.M., Khan, J.M., Curry, B.P. and Fortner, R.J., Phys. Rev.Letters 21 (1968) 1731.
4) Brandt, W. and Laubert, R., Phys.Rev.Letters 24 (1970) 1037.
5) Cairns, J.A., Holloway, D.F. and Nelson, R.S., Atomic Collision Phenomena in Solids (edited by D.W. Palmer, M.W. Thompson and P.D. Townsend, North-Holland Publ.Comp., Amsterdam).
6) Nelson, R.S., Defects in crystalline solids (edited by S. Amelinckx, R. Gevers, J. Nihoul, North-Holland Publ.Comp., Amsterdam 1968) Vol. I.
7) Mayer, J.W., Eriksson, L. and Davies, J.A., Ion Implantation in Semiconductors (Academic Press, New York 1970).
8) Saris, F.W., Weg, W.F. v.d. and Onderdelinden, D., Rad.Effects 1 (1969) 137.
9) Onderdelinden, D., thesis, Leiden 1968.
10) Saris, F.W. and Onderdelinden, D., Physica 49 (1970) 441.
11) Richard, P., Bonner, T.I., Furuta, T. and Morgan, I.L., Phys.Rev. A, 1 (1970) 1044.
12) Needham, P.B. Jr. and Sartwell, B.D., Phys.Rev. A, 2 (1970) 27.
13) Saris, F.W., Physica to be published.
14) Nielsen, K.O., in: "Electromagnetically Enriched Isotopes and Mass Spectroscopy" (edited by M.L. Smith, Academic Press, New York 1956) p.68.
15) Haensel, R., Kunz, G., Sasaki, T. and Sonntag, B., Appl.Opt. 7 (1968) 301.
16) Almén, O. and Bruce, G., Nucl.Inst.& Meth. 11 (1961) 257.
17) Behrisch, R.M., Ergebnisse der Exakten Naturwissenschaften (edited by S. Flügge and F. Trendelenburg, Springer Verlag, Berlin 1964) p.235.
18) see for instance Bohr, N. and Lindhard, J., Dan.Mat.Fys.Medd. 28 (1954) no.7.
19) Lindhard, J., Dan.Mat.Fys.Medd. 34 (1965) no.14.
20) Andreasen, O., Andersen, J.U. and Davies, J.A., Int.Conf.on Ion Implantation (Thousand Oaks, 1970) to be published.
21) Eriksson, L., Phys.Rev. 161 (1967) 235.
22) Carter, G. and Colligon, J.S., Ion Bombardment of Solids (American Elsevier, New York, 1968).
23) McCaughey, M.P., Knystautas, E.J., Hayden, H.C. and Everhart, E., Phys.Rev. Letters 21 (1968) 65.
24) Ogurtsov, G.N., Flaks, I.P. and Avakyan, S.W., Proceedings of the VI ICPEAC (edited by I. Amdur, MIT Press, Cambridge 1969) p.274.
25) Kistemaker, J. and Sanders, J.B., Proceedings 2nd L.H. Gray Conf. (Trinity College, Cambridge, 1969).

CHAPTER V

CONCLUSIONS AND POSSIBLE EXTENSIONS

"Sollten nun die neuen Strahlen nicht longitudinalen Schwingungen im Äther zuzuschreiben sein?"

W.C. Röntgen, 1895.

1. We have been able to detect Ar L-shell X-rays in collisions of various ions on Ar, thus proving that innershell vacancies are produced. Two years ago this conclusion would not have sounded so trivial as it does today, because other ways of investigating ion-atom collisions have not been so indicative [1]. From the measured cross sections for X-ray emission we inferred critical internuclear distances for innershell excitation by using a semi-empirical model. These critical internuclear distances along with the cross sections show a strong oscillatory dependence on the atomic number Z of the collision partner. This can be considered as a geometrical effect of the sizes of the innershells involved. However, these data urge for an evaluation of the Fano-Lichten model [2] for asymmetrical systems.

2. It has been shown that the probability of a radiative decay (the fluorescence yield) can be deduced from ion-atom collision processes. This method is particularly important for the regions where the fluorescence yield is still unknown: the K-shells of elements with low

atomic number, and for the outershells [3]. In addition we can conclude from our experiments that the fluorescence yield is dependent upon the degree of excitation and ionization of the outershell during the collision. In this respect a useful scattering experiment would be to measure characteristic X-rays in coincidence with scattered ions of which the scattering angle, energy and charge state are determined.

3. In consequence of the latter conclusion a strong correlation between outershell excitation/ionization and characteristic X-ray generation is anticipated leading to a shift of the Z oscillations mentioned under 1. For instance, in chapter III, we observe that at higher impact energies the Ar-L X-ray emission cross section in collisions of Ti^+ on Ar rises above that of Ar^+ on Ar. This may be explained by a higher degree of excitation of the Ar M-shell by Ti^+ impact than by Ar^+ impact. It has been found recently that also in small angle scattering experiments [4] the inelastic energy lost in collisions of Ti^+ on Ar is higher than in Ar^+ on Ar. An exclusive experiment would be to determine the Auger excitation cross sections.

4. In chapter IV we already discussed that not only the deexcitation probability is increased but also the probability of an innershell electron promotion if the degree of ionization of the outershell is increased.

This is important to realize if one uses solid targets in measuring X-ray emission cross sections. Outershell ionization is caused by the successive collisions of the projectile as it is slowing down in the solid target. The degree of ionization depends on the projectile velocity and on the kind of projectile and target atom. Therefore it should be elaborated [7] in how much the observed Z-oscillations of the X-ray emission cross sections [5] coincide with the wellknown Z-oscillations of the electronic stopping power [6].

REFERENCES

1) See the review article of Kessel, Q.C. in Case Studies in Atomic Collision Physics I, edited by E.W. McDaniel and M.R. McDowell, North-Holland Publ. Comp. (Amsterdam, 1969).
2) Fano, U. and Lichten, W., Phys.Rev.Letters 14 (1965) 484.
3) Fink, R.W., Jopson, R.C., Mark, H. and Swift, C.D., Rev.Mod.Phys. 38 (1966) 513.
4) Bierman, D.J. and Turkenburg, W., private communication.
5) Chapter III;
Specht, H.J., Z.Phys. 185 (1965) 301;
Cairns, J.A., Holloway, D.F. and Nelson, R.S. in Atomic Collision Phenomena in Solids, edited by D.W. Palmer, M.W. Thompson, P.D. Townsend, North-Holland Publ.Comp. (Amsterdam, 1970) p.541;
Kavanagh, T.M., Cunningham, M.E., Der, R.C., Fortner, R.J., Khan, J.M., Zaharis, E.J. and Garcia, J.D., Phys.Rev.Letters 25 (1970) 1473.
6) Mayer, J.W., Eriksson, L. and Davies, J.A., Ion Implantation in Semiconductors (Academic Press, New York, 1970) p.51.
7) Saris, F.W. and Bierman, D.J., to be published in Phys.Letters.

SAMENVATTING

Dit proefschrift omvat een studie van de produktie van karakteristieke röntgenstralen tijdens heftige botsingen tussen ionen en atomen. Het is reeds enige jaren bekend dat door een dergelijke botsing een of meer binnenschil elektronen aangeslagen kunnen worden. Het ontstaan van een binnenschil gat geeft aanleiding tot twee concurrerende processen: een Auger-proces waarbij een of meer snelle elektronen worden uitgezonden, of een elektron overgang waarbij de vrijkomende energie wordt uitgestraald in de vorm van een röntgenfoton. De detectie en analyse van deze röntgenfotonen geeft enig inzicht in het elektron excitatie- en deexcitatie mechanisme bij ion-atoom botsingen.

In hoofdstuk I wordt naast een algemene inleiding ook een overzicht gegeven van de literatuur over het onderwerp van dit proefschrift. Aan de orde komen de belangrijkste conclusies, met betrekking tot atomaire botsingsprocessen, waartoe het onderzoek naar de röntgenemissie in de laatste paar jaren heeft geleid. Aangezien dit onderzoek reeds aanleiding heeft gegeven tot enkele toepassingen buiten het gebied van het zuivere atomaire botsingsonderzoek wordt ook hier enige aandacht aan besteed.

De binnenschil excitatie bij ion-atoom botsingen is uitvoerig bestudeerd met behulp van verstrooiingsexperimenten van Ar^+ aan Ar en Ne^+ aan Ne. Voor deze systemen heeft men ook Auger-elektronemissie waargenomen, afkomstig van stralingsloze overgangen naar gaten in de Ar L-schil en Ne K-schil. In aansluiting hierop zijn wij gestart met een onderzoek naar de karakteristieke röntgenemissie bij botsingen tussen Ar^+,

Ne^+, H^+ op Ar en Ne^+ op Ne, zie hoofdstuk II.
Bij deze experimenten wordt een gasvormig doelwit beschoten met een naar massa en energie geanalyseerde ionenbundel in het energiegebied van enkele keV's tot 140 keV.
De röntgenfotonen worden waargenomen met behulp van een proportionele telbuis. Het blijkt relatief eenvoudig te zijn om met deze apparatuur absolute metingen te verrichten, zodat in hoofdstuk II de totale werkzame doorsneden gegeven worden voor Ar-L en Ne-K fotonemissie in de bovengenoemde botsingen. Een vergelijking tussen de werkzame doorsneden voor röntgenemissie en die voor Auger-elektronemissie levert de zogenaamde fluorescentie opbrengst op. Uit onze experimenten is gebleken dat deze fluorescentie opbrengst sterk afhankelijk is van de excitatie/ionisatie graad van de buitenschil. De werkzame doorsneden voor het geval van proton bombardement zijn enkele ordes van grootte kleiner dan die voor de beschieting met zwaardere ionen, waarmee wordt aangetoond dat het aanslag mechanisme voor deze gevallen essentieel verschillend is. Teneinde de invloed van het soort projectiel verder te onderzoeken hebben wij de totale werkzame doorsneden bepaald voor Ar-L fotonemissie in botsingen van He^+, C^+, N^+, O^+, Ne^+, Al^+, Cl^+, Ti^+, Fe^+, Cu^+ op Ar, zie hoofdstuk III. Met behulp van een semi-empirisch model voor binnenschil excitatie wordt uit de drempelenergie voor de röntgenemissie afgeleid de kritische afstand van dichtste nadering voor de Ar L-schil excitatie bij de ion-atoom botsing. Het blijkt dat deze kritische internucleaire afstand evenals de werkzame doorsnede sterk afhankelijk is van het atoomgetal van het projectiel.

Onze experimenten, zoals beschreven in de hoofdstukken II en III, onderscheiden zich van die van andere auteurs in zoverre, dat tot voor kort alleen gebruik gemaakt werd van metalen trefplaatjes terwijl wij een gasvormig doelwit toepasten. In hoofdstuk IV daarentegen wordt een beschrijving gegeven van een onderzoek naar de produktie van karakteristieke röntgenstralen bij Ar^+ en Ne^+ beschieting van monokristallijn koper. De absolute stralingsopbrengst is gemeten als functie van de primaire energie van de invallende ionen tussen 30 keV en 100 keV. Het vergelijken van de intensiteit met die bij botsingen in de gasfase stuit op moeilijkheden die inherent zijn aan het gebruik van een zeer dicht target. Ook werd waargenomen dat de intensiteit van de uitgezonden Ar-L straling afhankelijk is van het aantal ingeschoten argon ionen, waarmee wordt aangetoond dat deze straling afkomstig is van zowel Ar + Cu botsingen als Ar + Ar botsingen in het koperrooster. Hetzelfde effect treedt op bij Ne^+ beschieting. Wij hebben ook de stralingsopbrengst gemeten als functie van de hoek van inval van de ionenbundel ten opzichte van de kristaloriëntatie van het trefplaatje. Deze metingen geven enig inzicht in het binnendringen en begraven van de ionen in de vaste stof.

Tot slot worden in hoofdstuk V puntsgewijs een aantal conclusies genoemd die volgen uit het in het proefschrift beschreven werk. Hieraan worden ook enige suggesties toegevoegd voor nieuwe experimenten in dit nog grotendeels braakliggende terrein van onderzoek.

Tot slot een kort overzicht van mijn studie en een woord van dank aan diegenen die hebben meegewerkt aan het tot stand komen van dit proefschrift.

Na het behalen van het einddiploma H.B.S.-B aan het St.Nicolaaslyceum te Amsterdam, begon ik in september 1960 mijn studie aan de Universiteit van Amsterdam. Het kandidaatsexamen in de wiskunde en natuurkunde met sterrenkunde legde ik in december 1963 af, waarna het doctoraalexamen hoofdvak natuurkunde uitgebreid (hoofdrichting experimentele natuurkunde) volgde in maart 1967. Sinds februari 1964 ben ik verbonden aan het FOM-Instituut voor Atoom- en Molecuulfysica te Amsterdam, eerst als wetenschappelijk assistent en na het doctoraalexamen als wetenschappelijk medewerker.

De direkteur van dit instituut, professor dr. J. Kistemaker, ben ik zeer erkentelijk voor de stimulerende invloed die hij de afgelopen zeven jaar op mij heeft gehad. Als mijn promotor had hij zowel de goede intuïtie om het onderwerp van dit proefschrift voor te stellen, als de wetenschappelijke belangstelling om mijn werk kritisch te begeleiden. Ik dank professor dr. J. Los voor de vele waardevolle discussies en voor zijn bereidwilligheid om als medelezer op te treden. Professor dr. P.K. Rol en dr. D. Onderdelinden zijn mijn direkte leermeesters geweest. Onder Piet's inspirerende leiding heb ik gewerkt aan het onderwerp van mijn doctoraalverslag: "Kathodeverstuiving van f.c.c. kristallen". De discussies die ik vrijwel dagelijks met Dirk voerde zijn van doorslaggevende betekenis geweest voor het tot stand komen van dit proefschrift. Het intensieve kontakt met de leden van de "sputtergroep" heeft mijn werk aanzienlijk veraangenaamd. Ik dank vooral Werner van der Weg en Dick Bierman voor hun belangrijke bijdragen bij het interpreteren van de experimenten, en Simon Doorn en Huib Roukens voor de grote toewijding en nauwkeurigheid waarmee zij technische assistentie hebben verleend. Onmisbaar zijn de werkzaamheden geweest van de technische service groepen van het instituut. Voor hun medewerking dank ik: E. de Haas en de constructeurs, A. Neuteboom en de instrumentmakers, P. van Deenen en de elektronici en in het bijzonder G. Frijlink met wie ik gedurende twee jaren het vacuümlaboratorium leidde. Voor hulp bij vele administratieve problemen wil ik mevrouw A. Klapmuts en mevrouw L. Roos bedanken.

Voor dit proefschrift is het typografisch werk verzorgd door mevrouw C. Köke-van der Veer, het fotografisch werk door de heren F. Monterie en Th. van Dijk, het drukwerk door de heer H. Luyten. Ik ben hen allen veel dank verschuldigd.